Cancer Biol Med 2026. doi: 10.20892/j.issn.2095-3941.2025.0323

ORIGINAL ARTICLE

OPEN ACCESS

# FDX1 expression promotes DSF/Cu-induced cuproptosis in gastric cancer cells

Qirong Li[1], Yi Guo[2], Jiahuan Yuan[1], Qiang Feng[1], Hengzong Zhou[1], Ming Hao[3], Boqiang Tao[3], Liqun Sun[4], Chao Lin[5], Jianfeng Mu[6], Gongliang Guo[7], Dongxu Wang[1]

[1]Laboratory Animal Center, College of Animal Science, Jilin University, Changchun 130000, China; [2]The Third Affiliated Hospital of Changchun University of Chinese Medicine, Changchun 130000, China; [3]Department of Oral and Maxillofacial Surgery, School and Hospital of Stomatology, Jilin University, Changchun 130000, China; [4]Outpatient Department of Pediatrics, Children's Medical Center, The First Hospital of Jilin University, Changchun 130000, China; [5]Animal Science Department, School of Grain Engineering and Nutritional Science, Jilin Business and Technology College, Changchun 130000, China; [6]Department of Gastric and Colorectal Surgery, General Surgery Center, The First Hospital of Jilin University, Changchun 130000, China; [7]Department of Cardiology, China-Japan Union Hospital of Jilin University, Changchun 130000, China

**ABSTRACT**

**Objective:** Gastric cancer (GC) is a prevalent malignant tumor that warrants the development of drugs and therapeutic targets. Cuproptosis has emerged as a promising mechanism by which to inhibit tumors because copper homeostasis disorders frequently occur in various malignancies. The combination of disulfiram (DSF) and copper ions (DSF/Cu) has been shown to have significant antitumor effects. This study utilized DSF/Cu to investigate the mechanism underlying cuproptosis in GC cells.

**Methods:** GC cells were treated with DSF/Cu and protein sequencing was performed to screen for differentially expressed genes. The mechanism by which overexpressed *FDX1* regulates cuproptosis and *WDR43* expression was determined. Subsequently, how to improve the efficacy of DSF/Cu in the treatment of GC was studied in a mouse model of GC.

**Results:** DSF/Cu had a good therapeutic effect on promoting cuproptosis in GC cells. Protein sequencing revealed *WDR43* as a downstream gene of *FDX1*. Increasing the expression of *FDX1* enhanced the sensitivity of GC cells to copper treatment and inhibited the expression of *WDR43*, thereby exerting an antitumor effect. Furthermore, DSF/Cu was loaded into exosomes derived from natural killer (NK) cells to enhance the biological safety and tumor targeting of DSF/Cu and validate the inhibitory effect on GC both *in vitro* and *in vivo*.

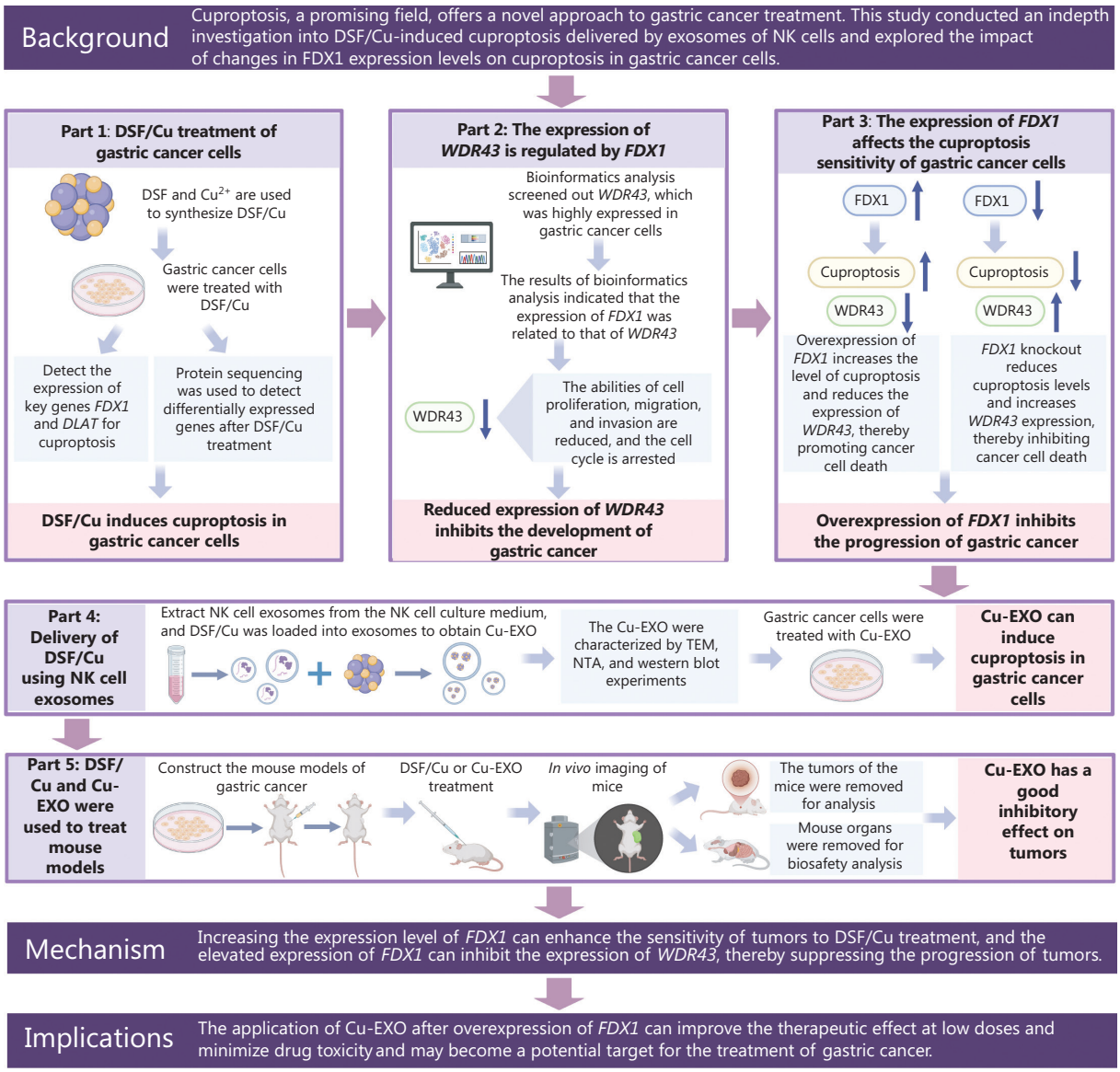
**Conclusions:** This study showed that DSF/Cu promoted cuproptosis and the expression of *FDX1* affected cuproptosis sensitivity of GC. Moreover, the combination of NK cell exosomes with DSF/Cu improved the therapeutic effect of DSF/Cu, which helps to promote the targeted therapy of GC and improve clinical applicability.

**KEYWORDS** Cuproptosis; gastric cancer; DSF/Cu; NK cell exosomes; *FDX1*

## Introduction

Copper (Cu) is an essential cofactor in the biological systems of all organisms. However, exceeding the Cu concentration threshold controlled by evolutionarily conserved homeostatic mechanism can result in Cu toxicity[1]. A recent study that has attracted significant attention unveiled the mechanism by which Cu induces cell death. Cu-dependent regulated cell death introduces a novel pathway distinct from known mechanisms, relying on mitochondrial respiration. Researchers have identified that this process involves Cu binding directly to a lipoylated component within the tricarboxylic acid (TCA) cycle. This interaction leads to the aggregation of lipoylated proteins and subsequent loss of iron-sulfur clusters, inducing protein-toxic stress and ultimately resulting in cell death. This previously unrecognized form of cell demise is now referred to as cuproptosis[2]. Cancer cells, including lung adenocarcinoma, hepatocellular carcinoma, glioblastoma, colorectal cancer (CRC), breast cancer, gastric cancer (GC), are known to be regulated by cuproptosis[3]. Studies have shown a significant association between the presence of ferredoxin 1 (*FDX1*) and lipidated proteins, like dihydrolipoamide S-acetyltransferase

Correspondence to: Gongliang Guo and Dongxu Wang
E-mail: docg@jlu.edu.cn and wang_dong_xu@jlu.edu.cn
ORCID ID: https://orcid.org/0009-0000-7163-6581 and https://orcid.org/0000-0003-0464-1596
Received July 9, 2025; accepted June 2, 2026;
published online July 28, 2026.
Available at www.cancerbiomed.org
©2026 The Authors. Creative Commons Attribution-NonCommercial 4.0 International License (CC BY-NC 4.0)




**StudyFlow** Part 1 demonstrates that synthesized DSF/Cu functions to promote cuproptosis in gastric cancer (GC) cells. In Part 2, the differentially expressed gene, *WDR43*, was screened by protein sequencing. *WDR43* expression was shown to be related to *FDX1* expression and decreased *WDR43* expression inhibited the development of GC. Part 3 demonstrates that *FDX1* overexpression enhanced the sensitivity of GC cells to DSF/Cu treatment and promoted the death of GC cells by reducing *WDR43* expression. In Part 4, Cu-EXO was synthesized and shown to have a good effect on promoting the death of GC cells. In Part 5, after constructing a mouse model of GC and applying Cu-EXO for treatment, Cu-EXO was shown to have good therapeutic effects and biological safety. DSF, disulfiram; Cu-EXO, exosomes loaded with DSF/Cu.

(DLAT) and lipoic acid synthetase (LIAS), in different human tumors. Moreover, cell lines with higher levels of lipidated proteins exhibit sensitivity to cuproptosis, indicating that targeting the Cu ionophore could be a promising approach for treating tumors with this specific metabolic characteristic[2]. Previous studies have shown through bioinformatics analysis that *FDX1*, *LIAS*, and *MTF1* are key genes that promote cuproptosis treatment and may be regarded as biomarkers for GC patients[4].

Proteins containing the tryptophan-aspartate repeat (WDR) domain are involved in cellular processes, such as signal transduction, transcriptional regulation, cell cycle control, cytoskeleton assembly, and chromatin modification[5]. The WDR repeat domain 43 (WDR43) protein belongs to a family of proteins containing the WDR domain, which has a key role in ribosome biogenesis and it has been shown that *WDR43* can induce the expression of cyclin[6]. In addition, *WDR43* is highly expressed in clinical samples of CRC patients and can

serve as a valuable biomarker for the diagnosis and treatment of CRC[7]. Another study showed that *WDR43* overexpression promotes the progression of CRC, while *WDR43* knockdown significantly inhibits cell growth by blocking the cell cycle and enhancing the effects of oxaliplatin chemotherapy[8]. Our research findings revealed that *FDX1* regulates the expression of *WDR43*, thus *WDR43* may become a potential therapeutic target for cancer.

GC is currently the fifth most common malignant tumor worldwide and ranks as the third leading cause of cancer-related deaths globally. Early diagnosis rates for GC remain low[9]. Among the current clinical treatment methods available for GC patients, surgery is the only method that can completely eradicate GC and is also the foundation for GC treatment. Adjuvant treatments, including combined chemotherapy, radiotherapy, molecular targeted therapy and immunotherapy, can improve the survival rate of patients with GC[10]. However, these treatments often come with serious side effects and suboptimal therapeutic outcomes, highlighting the need for new therapeutic approaches[11]. One promising option is the thiolam derivative, disulfiram (DSF), which acts as a Cu ionophore and has shown significant antitumor activity against various cancers, including GC, prostate cancer, glioma, and breast cancer[12]. Notably, the combined application of DSF and Cu ion (DSF/Cu) at the tumor site has been shown to enhance the therapeutic efficacy of DSF in GC[13]. Research has demonstrated that DSF/Cu can trigger antitumor effects in GC by activating the reactive oxygen species (ROS)/mitogen-activated protein kinase (MAPK) and nuclear protein localization protein 4 (NPL4) pathways[14]. This research focused on investigating the mechanism underlying cuproptosis induced by DSF/Cu in cancer cells by analyzing the expression pattern of *FDX1* in GC. The study aimed to determine whether alterations in FDX1 expression impact the sensitivity of GC cells to DSF/Cu treatment with the ultimate goal of identifying improved strategies for inhibiting cancer through DSF/Cu therapy.

The concentration of Cu ion at the tumor site needs to reach a certain level to inhibit tumors[15]. However, excessive oral Cu ion will cause systemic toxicity to the body, which seriously hinders the application of DSF/Cu in clinical tumor treatment[16]. Therefore, there is a need to develop a drug delivery method that can enhance tumor sensitivity to Cu ions at the site and improve chemotherapy outcomes with lower doses of Cu ions. Exosomes are extracellular vesicles with bilayer membrane structures released by cells. Exosomes can transport proteins, lipids, and RNAs, facilitating communication between different cell types in the body and demonstrating excellent biocompatibility[17]. Natural killer (NK) cells have a crucial role in the innate immune system, serving as primary defenders against cancer and pathogens[18]. Exosomes derived from NK cells demonstrate superior stability, greater potential for modification, and lower immunogenicity compared to NK cells[19]. In addition, NK cell-derived exosomes contain important cytotoxic proteins, like perforin (PFN), granzyme A (Gzm-A), granzyme B (Gzm-B), and granulysin (GNLY), which contribute to the cytotoxic effects[20]. Studies have shown that NK cell-derived exosomes can boost the proliferation of NK cells and display cytotoxicity against hematologic cancers and breast cancer[21]. As a result, NK cell exosomes show promise as a novel therapeutic strategy for treating GC.

NK cell exosomes were utilized to deliver DSF/Cu (Cu-EXO) to modulate *FDX1* expression in GC cells and investigate the *FDX1*/*WDR43* axis. This strategy effectively improved the therapeutic effectiveness of DSF/Cu against GC cells and inhibited tumor growth through cuproptosis.

# Material and method

## Cell culture and DSF/Cu treatment

Epithelial cells of the human stomach (GES1), as well as two types of cells found in human GC (MKN45 and AGS) were incubated in RPMI-1640 medium containing 10% fetal bovine serum [FBS] (Gibco, Grand Island, New York, USA) at 37°C in 5% $CO_2$. A combination of DSF/Cu at a 1:1 ratio was administered to the GES1, MKN45, and AGS cell lines upon reaching a cell growth density of 80%–90% and allowed to incubate for 24–48 h. All human cell lines have been authenticated using STR profiling all experiments were performed with mycoplasma-free cells.

## RNA extraction and gene expression analysis

GC cells were treated with DSF/Cu for 24 h, after which the cells were collected and total RNA was extracted. Conversion of RNA into cDNA was performed using the first strand cDNA synthesis kit (Tiangen, Beijing, China). Real-time quantitative polymerase chain reaction (qPCR) was used to assess the levels of *FDX1*, *DLAT*, *LIAS*, and *WDR43* expression. The qPCR conditions included the following: an initial heating at 94°C for 3 min; followed by 35 cycles of denaturation at 94°C for 10 s, annealing at 59°C for 15 s, and extension at 72°C for 30 s. β-actin was used as the control gene. The primer sequences are provided in **Table S1**.

## Western blot

Total proteins were extracted from GC cells with Beyotime extraction buffer using the BCA protein assay kit (Tiangen) for quantification. The subsequent process included separating the proteins through SDS-PAGE, transferring the proteins onto a PVDF membrane, and combining the membrane with primary antibodies against FDX1, DLAT, WDR43, cyclin dependent-kinase 2 (CDK2), cyclinD-1, and β-actin (Proteintech, Wuhan, China). These primary antibodies were allowed to incubate overnight at 4°C. Subsequently, secondary antibodies (goat anti-rabbit) were introduced, diluted to

1:10,000, and left to incubate at 37°C for 1 h. The resulting bands were then subjected to analysis using ECL Super Signal (Pierce, Rockford, Illinois, USA).

## Proteomic analysis

Total proteins of DSF/Cu-treated GC cells were extracted for protein sequencing and peptides were separated by reverse-phase high-performance liquid chromatography (RPLC). After peptide enrichment, liquid chromatography-mass spectrometry tandem analysis was performed for MS data processing and analysis. After obtaining the results of quantitative and qualitative analysis of proteins, bioinformatics analysis was performed using omics data analysis tools. The target proteins with FDX1 regulatory effects were screened and verified.

## Knockout and overexpression of FDX1 gene and knockdown of WDR43

The vector for FDX1 overexpression was built utilizing pcDNA3.1 (GenePharma, Suzhou, China). Concurrently, the FDX1 knockout (KO) vector was formulated using the CRISPR/Cas9 framework (px459; (Addgene, Watertown, Massachusetts, USA). GC cells were transfected separately for 48 h with the FDX1 overexpression (pcDNA3.1) and FDX1-KO vectors. Cells transfected with non-specific pcDNA3.1-CON were used as controls. siWDR43 was obtained from RiboBio (Guangzhou, China). GC cells were transfected with siWDR43 for 48 h and control cells were transfected with non-specific siRNA.

## Protein-protein interaction

The crystal structures corresponding to the two proteins were obtained from the AlphaFold database. Protein pretreatment, natural ligand state regeneration, hydrogen bond allocation optimization, protein energy minimization, and water removal treatment were performed on the obtained protein structures. Protein-protein interaction simulations of the processed proteins using a protein-protein docking module were used to determine the specific part of the FDX1 binding to WDR43. The different chains of the protein-protein interaction complex and the lowest interaction fraction are labeled with different colors.

## Protein stability testing

To determine whether the protein half-life of WDR43 is altered upon FDX1 overexpression, transfected cells were treated with 50 μg/mL cycloheximide (CHX) at designated time points (0, 6, 12, and 24 h), followed by western blot analysis. FDX1-overexpressing cells were treated with 20 μM MG132 or 50 μM chloroquine (CQ) to determine whether the FDX1-mediated downregulation of WDR43 protein is associated with the ubiquitin-proteasome degradation pathway and subsequent western blot analysis was performed.

## NK cell identification

NK cells (Jilin Zhongke, Changchun, China) were harvested and rinsed two times using PBS. The cell count was reduced to $10^6$/100 μL with a 0.1% bovine serum albumin (BSA) solution. Subsequently, 5–10 μL of CD3, CD16, and CD56 antibodies (Invitrogen, Carlsbad, California, USA) were included and incubated at ambient temperature for 30 min. Finally, the cells were spun down and rinsed two times with PBS before being examined using flow cytometry (BD Biosciences, San Jose, California, USA).

## Acquisition of Cu-EXO

NK cells were maintained in NK cell culture medium containing 10% FBS at 37°C in 5% $CO_2$. The cell culture supernatants were harvested after 72 h. Exosomes were isolated using a series of ultra-fast centrifugation steps at 4°C, including spins at 300 g for 30 min, 2,000 *g* for 30 min, 12,000 *g* for 45 min, and finally at 110,000 g for 70 min post-filtration through a 0.22-μm membrane. After discarding the supernatant, the pellet was resuspended in PBS and underwent an additional spin at 110,000 *g* for 70 min. Subsequently, the NK cell exosomes were suspended in PBS and loaded with DSF/Cu using a freeze-thaw technique before being stored at −80°C. The quantity of exosomal proteins was assessed using a BCA protein analysis kit to determine the exosome concentration from NK cells. The Cu ion level within the exosomes was measured with a Copper Ion Content Analysis Kit (Elabscience, Wuhan, China).

## Characterization of Cu-EXO

Cu-EXO was fixed with 2% PFA for 5 min. Then, the exosome suspension was placed in the grid and incubated for 10 min. The EM mesh surface was stained with 1% uranyl acetate (UA) solution for 2 min. The surplus UA solution is subsequently blotted from the mesh using filter paper and dried at room temperature. The morphology of exosomes was examined using transmission electron microscopy.

The particle size and concentration of exosomes were measured by nanoparticle tracking analysis (NTA) using an NanoFCM instrument (Flow NanoAnalyzer, Xiamen, China). The exosomes isolated by ultracentrifugation were diluted with 1 × PBS, then samples were sent for detection. After the instrument performance test with standard products was qualified, the exosome sample was loaded, and the sample gradient was diluted to avoid blocking the injection needle.

Total NK cell exosomal proteins were extracted and the expression of exosomal surface markers [TSG101 and CD9] (Abcam, Waltham, Massachusetts, USA) was detected by western blot analysis using the extracted NK cell culture medium as the control.

## Cell migration, invasion, proliferation, cycle analysis, and clonal formation

GC cells were treated or transfected with DSF/Cu, overexpressed vector, FDX1-KO vector, siWDR43, or Cu-EXO. The cells were cultured after being scratched in a serum-free medium. Images were taken after 0, 24, 48, and 72 h of culture, and the scratch area was used to express the cell migration rate.

Matrigel (BD Biosciences, San Jose, California, USA) and serum-free RPMI-1640 were diluted at a 1:8 ratio and added to a Transwell chamber (Corning Life Sciences, Tewksbury, Massachusetts, USA) until Matrigel solidified. Cells treated or transfected with DSF/Cu, overexpressed vector, FDX1-KO vector, siWDR43, or CU-EXO for 24–48 h were added to the cell at $10^5$ per 100 μL, filled with 0.5 mL medium containing 10% FBS outside the cell, incubated for 24 h, and fixed with 4% paraformaldehyde. Photographs were taken after staining with 0.1% crystal violet.

The proliferation activity of GC cells was measured after treatment or transfection with DSF/Cu, overexpressed vector, FDX1-KO vector, siWDR43, or Cu-EXO. The treated and the control cells were placed in 96-well plates and cultured in medium. After 24 h, CCK-8 reagent (Meilunbio, Dalian, China) was added and incubated for 0.5–4 h. OD values were obtained at 450 nm using an enzymoleter (Tecan, Männedorf, Switzerland).

GC cell samples treated or transfected with DSF/Cu, overexpressed vector, FDX1-KO, siWDR43, or Cu-EXO were selected with a Cell Cycle Detection Kit (Meilunbio, Dalian, China). After the cells were collected, the cells were fixed with 75% alcohol and the dyeing solution was mixed according to the ratio of dyeing buffer, as follows: propyl iodide (PI) dyeing solution:RNase A = 100:5:2. Each cell sample was added to 500 μL of staining solution, the cell precipitation was suspended, and the temperature bath was protected from light at 37°C for 30 min. BD flow cytometry was used to analyze whether the cell cycle was affected.

The 1,000 treated cells were cultured in a 6-cm dish. The fluid was changed every 3–5 d. The culture was completed after 2 weeks, fixed with 95% ethanol, and stained with 0.1% crystal violet. The stained cultures were allowed to dry and photographed, and the cell colonies were counted.

## Cell live/dead staining

Cell viability was analyzed using the Live/Dead Assay Kit (Abbkine, Wuhan, China). The treated cells were incubated in a dark environment with 0.5 mL of staining solution. Green fluorescence (live cells) and red fluorescence (dead cells) images were captured using a fluorescence microscope (Olympus, Hachioji, Japan).

## Immunofluorescence staining

After treatment, cells were fixed with 4% paraformaldehyde and washed with PBS. The cells were subsequently permeated with 1% BSA for 1 h, washed with PBS, and antibodies were added and incubated overnight at 4°C. The cells were washed three times, then the corresponding secondary antibody was added and incubated for 1 h. DAPI working solution was added and incubated in the dark for 15 min. Finally, the sample images were captured using a fluorescence microscope.

## *In vitro* tracking of exosomes

A DiO Kit (Meilunbio) was used to label exosomes and track the *in vitro* uptake of EVs, according to the manufacturer's procedures. Cells were cultured to 70%–80% fusion in a 6-well plate to determine whether EVs could be internalized by cells. Then, exosome-labeled exosomes were added and incubated with the cells for 8 h. Direct observation was performed with laser scanning confocal microscopy [LSCM] (Olympus).

## Small animal *in vivo* imaging

Exosomes were labeled to track the release of exosomes *in vivo* using a PKH-26 Kit (Beyotime, Shanghai, China) according to the manufacturer's protocol. The exosomes were incubated with 500 μL of diluted C solution and 4 μL of PKH-26 dye solution in a dark environment at room temperature for 5 min. Then, 500 μL of 1% bovine serum albumin was added to stop the staining. The labeled exosomes were obtained by super-centrifugation of 100,000 g for 70 min and suspension with 200 μL of PBS. After bearing tumor, nude mice were injected with PKH-26 labeled Cu-EXO. An equal amount of PBS was used as a control. Nude mice were anesthetized by inhalation with 2% isoflurane. Anesthetized mice were imaged using a Bioluminescence Imaging System ($\lambda_{ex}$ = 530 nm, $\lambda_{em}$ = 600 nm; Biolight Biotechnology, Guangzhou, China) within 2 h after injection.

## GC mouse model construction

Forty female nude mice (6–8 weeks old; Vital River, Beijing, China) were utilized for *in vivo* tests. Forty mice were randomly divided into 5 groups without bias. Mice were injected under the left ribcage with $8 \times 10^6$–$1 \times 10^7$ AGS cells or AGS cells overexpressing *FDX1*. The mice were administered DSF/Cu or Cu-EXO 7 d after the injection for a duration of 2 weeks. Mice weights were measured and documented. The control group was given a solution of solvent (DSMO) and PBS. The mice were euthanized on the 14th d of treatment, the tumor tissue was excised, the tumor dimensions were evaluated, and a histopathologic analysis was performed. The Cu ion content in the heart, liver, spleen, lungs, and kidney tissues was detected

using a Tissue Copper Ion Detection kit (Elabscience). Mice were euthanized by cervical dislocation. Another five groups of mice were treated as described above after tumor loading and the survival conditions were continuously observed and recorded for 160 days. The mice used in the experiment were obtained from the Laboratory Animal Center at Jilin University (Changchun, China) and were housed under SPF conditions. The mice were provided a standard rodent diet and water *ad libitum* within their cages. The study underwent review and approval by an Institutional Ethics Committee prior to start. The study protocol involving animals was sanctioned by the Institutional Animal Care and Use Committee of Jilin University (SY202306044). All procedures were carried out following the guidelines outlined in GB/T 35892-2018 for Laboratory Animals – Ethical Review Protocol and adhered to the ARRIVE guidelines.

### Hematoxylin and eosin (HE) staining

The tumor and organ tissues underwent fixation in 4% paraformaldehyde for a duration of 48 h, followed by a 24 h wash in PBS at 4°C. The sample was subsequently embedded in paraffin wax and sectioned into 5-mm thick slices. These sections were stained with HE, allowing for the observation of cancer cell infiltration under a microscope.

### Statistical analysis

An unpaired Student t-test and one-way ANOVA (Tukey's multiple comparisons test) were utilized in this study. SPSS 16.0 software was used for statistical analysis. Data are presented as the mean ± standard deviation. A $P$ value < 0.05 was regarded as statistically significant.

## Results

### DSF/Cu inhibited the growth of GC cells

A DSF/Cu compound was synthesized for cellular experiments. After the synthesis of the DSF/Cu complex, energy dispersive spectroscopy (EDS) elemental tests, Fourier transform infrared spectroscopy (FTIR) detection, and X-ray photoelectron spectroscopy (XPS) detection were performed to analyze the surface elemental composition, chemical composition, and molecular structure of the DSF/Cu complex (**Figure S1A–C**). Initially, GC cells were exposed to various concentrations of DSF/Cu and proliferation was assessed using the CCK-8 assay. Subsequent experiments utilized concentrations that exhibited a 50% inhibition rate (**Figure 1A**). GES1 cells were also treated with DSF/Cu; CCK-8 detection proved that DSF/Cu produced a killing effect on normal cells at a concentration of 3 μM (**Figure S2A**). Moreover, the clonogenic potential of GC cells post-DSF/Cu treatment was evaluated, showing a significant inhibition of GC cell clonogenesis (**Figure 1B**). The immunofluorescence results showed that the degree of DLAT aggregation increased after DSF/Cu treatment of GC cells (**Figure 1C**). These findings indicated that DSF/Cu effectively hinders GC cell proliferation and promotes the occurrence of cuproptosis. By investigating the expression of cuproptosis-related genes, elevated levels of FDX1 and DLAT proteins were demonstrated in GC cells compared to GES1, as confirmed by western blot analysis (**Figure 1D, E**). qPCR results also revealed increased *FDX1* and *DLAT* gene expression in AGS cells compared to GES1, while *LIAS* gene expression was decreased (**Figure 1F**). The above results demonstrated the patterns of key gene expression for cuproptosis in different GC cells. To distinguish DSF/Cu-induced cuproptosis from other cell death mechanisms, gene expression profiles associated with autophagy, ferroptosis, and apoptosis in GC cells post-treatment were analyzed. The qPCR data revealed no significant changes in the expression of these genes following DSF/Cu treatment (**Figure 1G–I**). After treating GC cells with the Cu chelator, TTM, the necrosis inhibitor, Nec-1, the ferroptosis inhibitor, Fer-1, the ROS inhibitor, NAC, and the apoptosis inhibitor, Z-VAD-FMK, the cells were subsequently treated with DSF/Cu. The CCK-8 assay revealed that only TTM treatment reversed inhibition of GC cell proliferation (**Figure S2B**). Western blot results indicated that TTM was the sole treatment altering the expression of cuproptosis-related genes (**Figure S2C**). Cell live/death experiments demonstrated that TTM effectively rescued cuproptosis induced by DSF/Cu (**Figure S2D**). Therefore, the results suggested that DSF/Cu induces cuproptosis in GC cells by modulating the expression of the cuproptosis-related gene, *FDX1*.

### Protein sequencing after DSF/Cu treatment of GC cells

Protein sequencing was performed on GC cells treated with DSF/Cu to determine the regulatory role of DSF/Cu-induced cuproptosis in GC cells. A total of 21 significantly differentially expressed proteins (DEPs) were identified with 4 proteins upregulated and 17 downregulated. Volcano plots and heatmaps visually represented the differentially expressed genes [DEGs] (**Figures 2A** and **S3A**). **Figure S3B** shows the sub-localization of DEGs in cells. Enrichment analysis of these proteins highlighted the involvement in cell surface signaling and cytokine-related pathways (**Figure 2B, C**). Gene Ontology (GO) and Cluster of Orthologous Groups (COG) analyses indicated that these genes were primarily associated with cellular processes and biological regulation (**Figure 2D, E**). Bioinformatic analysis revealed that the WDR43 protein was linked to the regulation of cellular component biogenesis and metabolic processes. WDR43 also had a significant correlation with the prognosis of GC patients (**Figure 2F**).

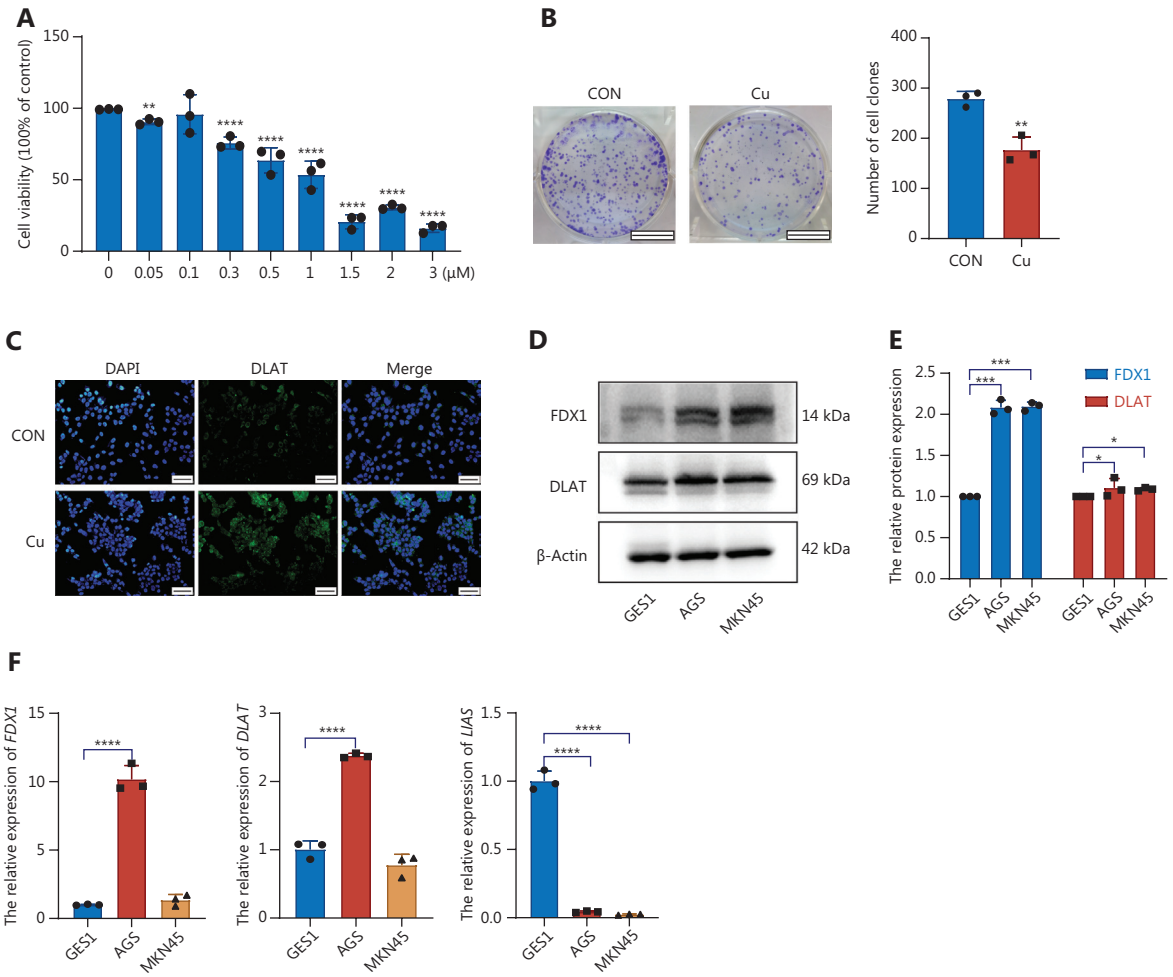



**Figure 1** Continued

Moreover, bioinformatics analysis showed that WDR43 was highly expressed in GC tissues (**Figure 2G**). The mass spectrum of WDR43 is presented in **Figure S3C**. Alphafold was utilized to predict the structure of the FDX1 protein with protein binding predictions indicating interaction sites between FDX1 and WDR43 proteins (**Figure S3D, E**). Point mutations were performed on the predicted binding sites (**Figure S4A–C**). The western blot results showed that when *FDX1* was overexpressed, the expression of WDR43 rebounded after simultaneous point mutations at all three sites (**Figure S4D**). The levels of *WDR43* expression in GC cells were assessed using qPCR and western blot techniques. The qPCR results revealed increased *WDR43* expression in GC cells compared to GES1 cells (**Figure 2H**), while DSF/Cu treatment resulted in increased *WDR43* expression in cancer cells (**Figure 2I**). Western blot analysis also confirmed high *WDR43* expression in GC cells (**Figure 2J, K**). These findings suggested a potential role for *WDR43* in the DSF/Cu-induced cuproptosis pathway in GC cells.

## Verifying the regulation of FDX1 on cuproptosis sensitivity of GC cells

Studies have shown that the level of cuproptosis-related genes may affect the occurrence of cuproptosis in cancer cells[22,23]. This study aimed to determine the impact of altering *FDX1* gene expression on the sensitivity of GC cells to DSF/Cu treatment and investigate the relationship between *FDX1* and *WDR43*. Overexpression and knockout vectors for *FDX1* were generated using the CRISPR/Cas9 system. qPCR analysis post-*FDX1* overexpression showed a significant increase in *FDX1* expression (**Figure 3A**). The CCK-8 assay revealed that DSF/Cu treatment after *FDX1* overexpression led to a notable inhibition of GC cell growth compared to DSF/Cu treatment alone (**Figure 3B**). Western blot analysis showed that *FDX1* expression increased, *WDR43* expression decreased, and the level of DLAT oligomerization increased after *FDX1* overexpression (**Figures 3C and S5A**). The protein half-life assay revealed that *FDX1* overexpression reduced the stability of WDR43 protein

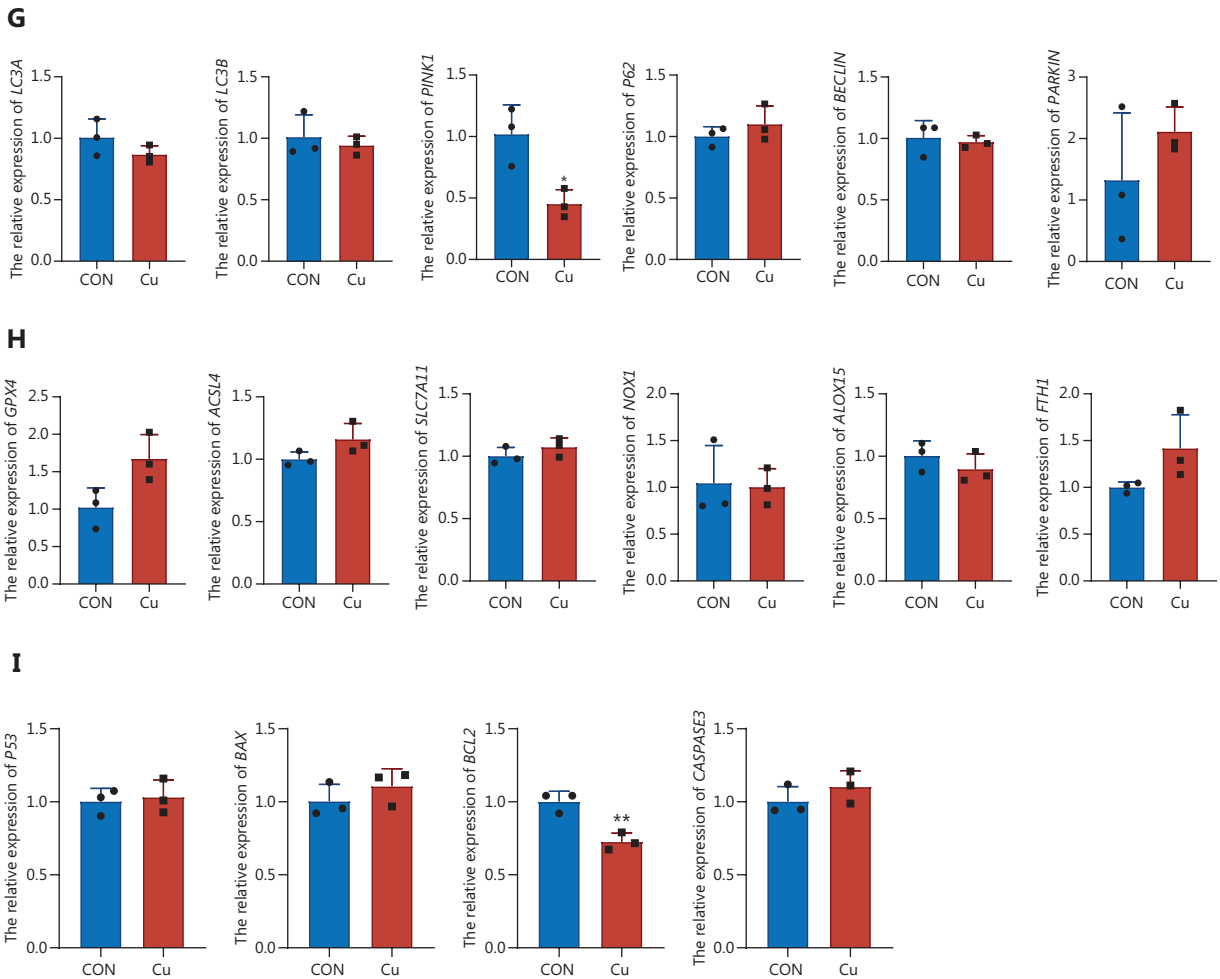



**Figure 1** Expression patterns of genes associated with cuproptosis in GC cells. (A) Cell proliferation after DSF/Cu treatment was detected by CCK-8 ($n$ = 3). (B) The clonogenesis ability of 1 μM DSF/Cu-treated cells for 24 h was detected by a plate cloning experiment ($n$ = 3) and statistical analysis of plate cloning results (scale bar, 10 mm). (C) Immunofluorescence assay ($n$ = 3) was used to detect oligomerization of DLAT in cells treated with 1 μM DSF/Cu for 24 h (scale bar, 50 μm). (D) Western blot detection of *FDX1* and *DLAT* gene expression levels in GES1, AGS, and MKN45 cells ($n$ = 3). (E) Statistical analysis of western blot. (F) qPCR was used to detect the levels of *FDX1*, *DLAT*, and *LIAS* gene expression in GES1, AGS, and MKN45 cells ($n$ = 3). (G) The levels of *LC3A*, *LC3B*, *PINK1*, *P62*, *BECLIN*, and *PARKIN* gene expression in GC-and DSF/Cu-treated GC cells were detected by qPCR ($n$ = 3). (H) The levels of *GPX4*, *ACSL4*, *SLC7A11*, *NOX1*, *ALOX15*, and *FTH1* gene expression in GC-and DSF/Cu-treated GC cells were detected by qPCR ($n$ = 3). (I) qPCR was used to detect the levels of *P53*, *BAX*, *BCL2*, and *CASPASE3* gene expression in GC-and DSF/Cu-treated GC cells ($n$ = 3). Data are expressed as the mean ± SD. *$P$ < 0.05, **$P$ < 0.01, ***$P$ < 0.001, and ****$P$ < 0.0001, indicating statistically significant differences.

and shortened the half-life (**Figure S6A, B**). After treatment of FDX1-overexpressing GC cells with MG132, FDX1-mediated downregulation of WDR43 protein was shown to be related to the proteasome degradation pathway (**Figure S6C, D**). Moreover, DSF/Cu treatment after *FDX1* overexpression reduced the migratory and invasive capabilities of GC cells (**Figure 3D–G**). In addition, *FDX1* overexpression induced G1 phase cell cycle arrest, while DSF/Cu treatment caused S phase cell cycle arrest (**Figure 3H, I**).

A CRISPR/Cas9 system was used to knock out *FDX1*, as shown in **Figure S7A, B**. Subsequent qPCR analysis confirmed the reduction in *FDX1* expression upon knockout, as depicted in **Figure 4A**. Interestingly, CCK-8 results revealed that the proliferation capacity of GC cells remained unaffected when *FDX1* was knocked out and DSF/Cu was added compared to DSF/Cu treatment alone (**Figure 4B**). Western blot experiments further demonstrated a decrease in *FDX1* expression, an increase in *WDR43* expression after *FDX1* knockout, and

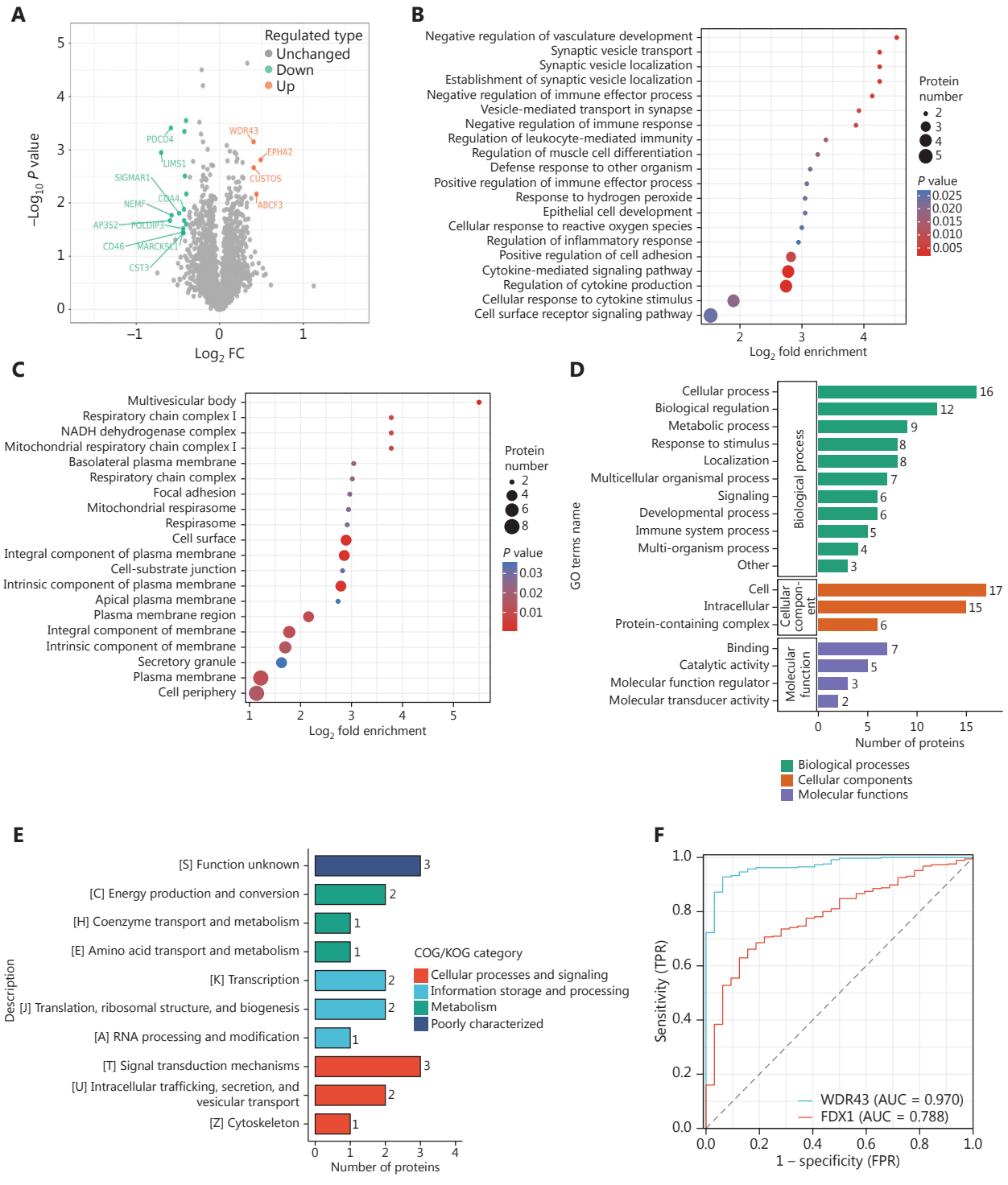



**Figure 2** Continued

the level of DLAT oligomerization decreased (**Figures 4C,S5B and S7C**). Notably, the migration and invasion abilities of GC cells were enhanced upon treatment with DSF/Cu following *FDX1* knockout (**Figure 4D–G**). Moreover, while DSF/Cu treatment led to cell cycle arrest in the S phase, knocking out *FDX1* did not significantly alter this effect (**Figure 4H, I**). These findings suggested that *FDX1* influences *WDR43* gene expression, the increase in *FDX1* expression leads to a decrease in *WDR43* expression in GC cells, and upregulation of *FDX1* can enhance the sensitivity of GC cells to DSF/Cu treatment.

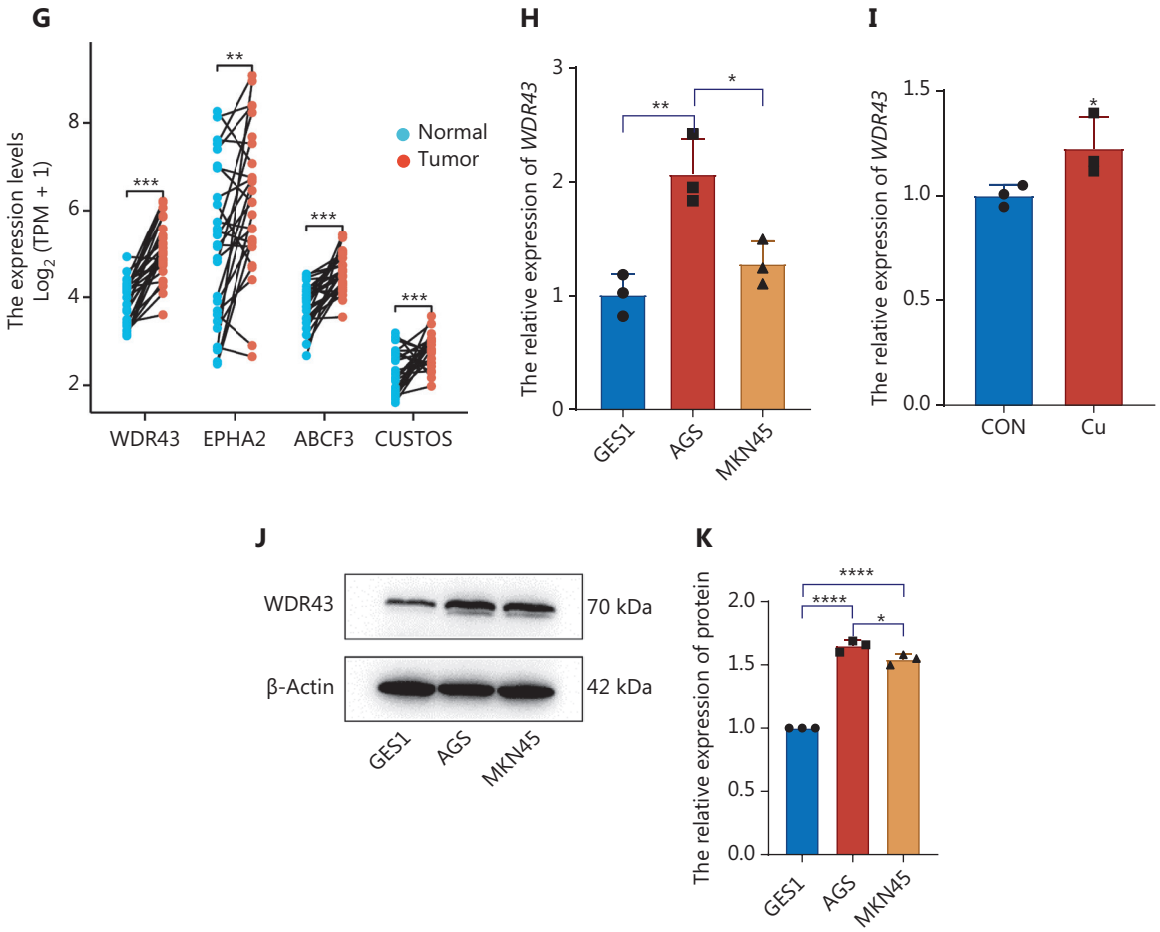



**Figure 2** Protein sequencing analysis of GC cells treated with DSF/Cu. (A) Volcano map analysis of differentially expressed proteins. (B) Protein domain enrichment analysis of biological process. (C) Protein domain enrichment analysis of cellular component. (D) GO annotation analysis. (E) COG/KOG functional classification analysis. (F) Prediction of the prognostic correlation between *FDX1* and *WDR43* in patients with GC. (G) Bioinformatics analysis predicts the expression of differentially expressed genes in GC tissues. (H) The level of *WDR43* expression in GES1, AGS, and MKN45 cells was detected by qPCR ($n$ = 3). (I) qPCR was used to detect the expression of *WDR43* in GC cells and 1 μM DSF/Cu-treated GC cells ($n$ = 3). (J) Western blot analysis of *WDR43* expression in GES1, AGS, and MKN45 cells ($n$ = 3). (K) Statistical analysis of western blot. Data are expressed as the mean ± SD. *$P$ < 0.05, **$P$ < 0.01, ***$P$ < 0.001, and ****$P$ < 0.0001 indicated statistically significant differences.

## Effects of decreased expression of WDR43 on GC cells

The current study aimed to determine the impact of changes in *WDR43* expression on GC cells because *WDR45* is a downstream gene of *FDX1* known to have an inverse relationship with *FDX1* expression. Following the synthesis of siWDR43 and knockdown of *WDR43*, western blot analysis confirmed a decrease in *WDR43* expression (**Figure 5A, B**). Subsequent CCK-8 assay results showed a reduction in the proliferation capacity of GC cells post-*WDR43* knockdown (**Figure 5C**). Moreover, decreased *WDR43* expression led to inhibition of invasion and migration abilities in GC cells (**Figure 5D–G**) and induced G1 phase cell cycle arrest (**Figure 5H, I**). Western blot analysis also revealed an upregulation of cell cycle-related proteins (CDK2 and cyclinD-1) with reduced *WDR43* expression (**Figure 5J, K**). In addition, the results of immunofluorescence and western blot indicated that the changes in *WDR43* expression did not affect the level of DLAT oligopolization (**Figure S8A, B**). Therefore, *WDR43* may not directly regulate the occurrence of cuproptosis in GC. These results indicated that downregulation of *WDR43* affects the growth of GC cells and suggested that the *FDX1*/*WDR43* axis has a crucial role in regulating cell cycle, migration, and invasion in these cells.

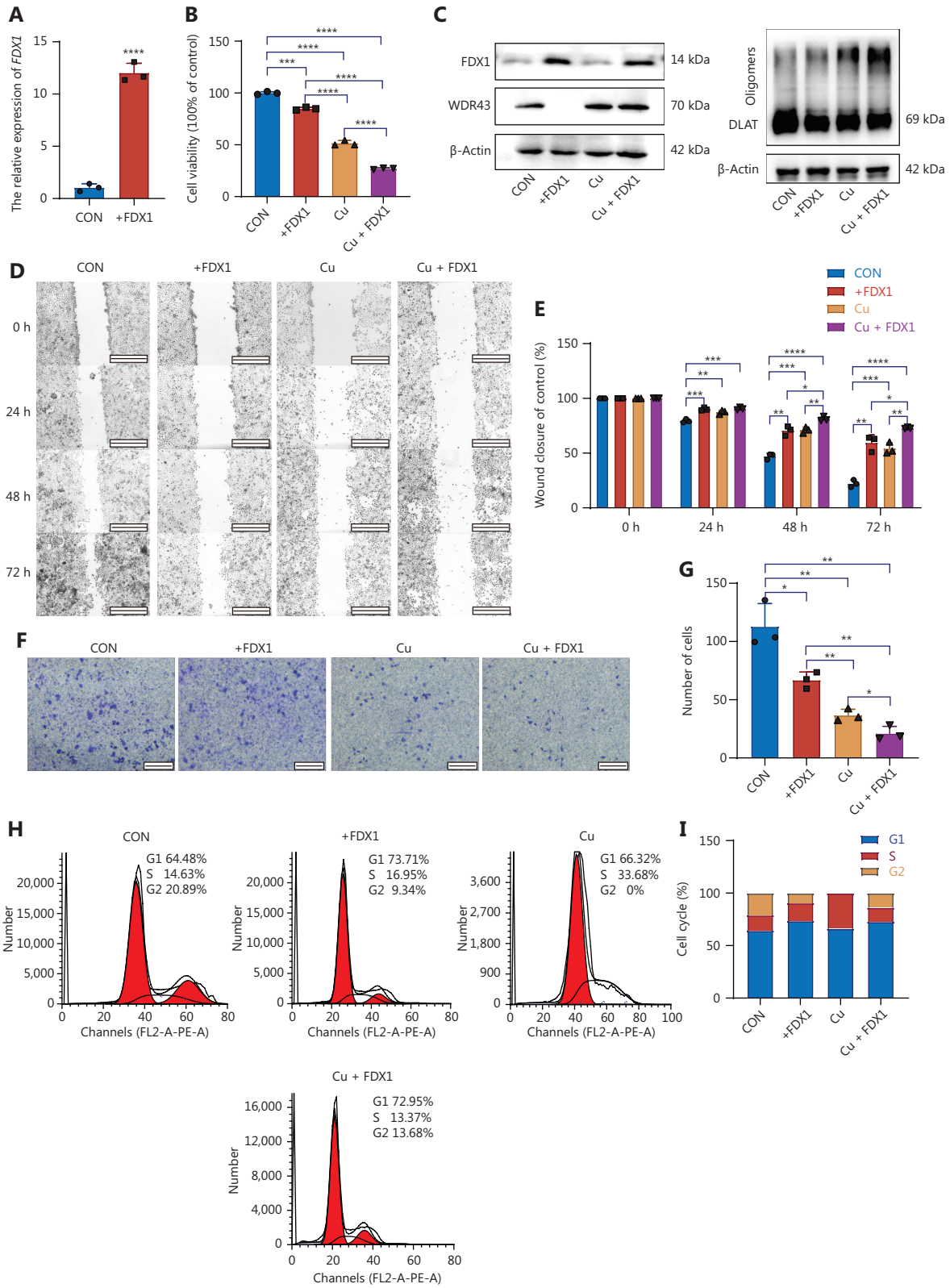



**Figure 3** Effects of *FDX1* overexpression on GC cells. (A) qPCR was used to detect the level of *FDX1* gene expression in overexpressed *FDX1* GC cells ($n$ = 3). (B) CCK-8 detected the proliferation of non-treated GC cells (CON), GC cells overexpressing *FDX1* (+FDX1), GC cells treated with 1 μM DSF/Cu for 24 h, and GC cells overexpressing *FDX1* and treated with DSF/Cu [Cu + FDX1] ($n$ = 3). (C) Western blot analysis of the

levels of FDX1, WDR43, and DLAT in *FDX1* overexpressed GC cells ($n$ = 3). (D) Scratch healing assay to detect cell migration ($n$ = 3) (scale bar, 500 μm). (E) Statistical analysis of the results of scratch healing experiments ($n$ = 3). (F) Invasion assay to detect the invasion ability of cells ($n$ = 3) (scale bar, 100 μm). (G) Statistical analysis of the results of invasion experiments ($n$ = 3). (H) Cell cycle was measured by flow cytometry ($n$ = 3). (I) Statistical analysis of cell cycle test results ($n$ = 3). Data are expressed as the mean ± SD. *$P$ < 0.05, **$P$ < 0.01, ***$P$ < 0.001, and ****$P$ < 0.0001, indicating statistically significant differences.

## DSF/Cu was loaded into NK cell exosomes to treat GC cells

DSF/Cu was encapsulated into NK cell exosomes, which are known for high biosafety, cellular uptake efficiency, and specific targeting abilities to further investigate enhancing the therapeutic potential of DSF/Cu. The efficacy of NK cell exosomes loaded with DSF/Cu (Cu-EXO) was evaluated *in vivo* and *in vitro*. Human NK cells were cultured (**Figure S9A**) and characterized by NK cell surface markers (**Figure S9B**). The exosomes were isolated and loaded with DSF/Cu. The morphology of Cu-EXO was examined using transmission electron microscopy (**Figure 6A**), while particle size analysis was performed to determine the size of Cu-EXO (**Figure 6B**). Exosome surface markers were identified through western blot analysis (**Figure 6C**). The concentration of $Cu^{2+}$ ion in Cu-EXO was quantified using a kit method (**Figure S10A**) and the treatment dosage of Cu-EXO was determined based on this ion concentration. The accuracy of the $Cu^{2+}$ ion content analysis kit method was verified through the spiking recovery experiment (**Figure S10B**) and it was confirmed by HPLC that DSF was also successfully loaded into exosomes (**Figure S10C**). Given the pivotal role of NK cells in immune regulation, the pro-inflammatory impact of Cu-EXO on GC cells was assessed using qPCR. The results indicated a reduction in the levels of inflammatory factor (TNF, IL-6, and IL-8) expression in GC cells following Cu-EXO treatment (**Figure S11A**). Subsequent experiments involving GC cells revealed that Cu-EXO significantly suppressed the proliferation of GC cells, supported by CCK-8 results (**Figure 6D**). Further analysis after Cu-EXO treatment showed a notable increase in *FDX1* expression and an increase in the level of DLAT oligomerization, as evidenced by qPCR and western blot results (**Figures 6E, F, and S11B**). In addition, treatment of GES1 and AGS cells with NK exosomes labeled with DiO dye demonstrated a higher affinity of NK exosomes towards GC cells, which led to internalization (**Figure S12A, B**). In addition, Cu-EXO treatment led to a reduction in migration ability, invasion rate, and induced cell cycle arrest among GC cells in the S phase (**Figure 6G–L**). These findings collectively suggested that Cu-EXO exhibits promising efficacy in inhibiting GC cell proliferation and inducing cuproptosis *in vitro*.

## Cu-EXO can inhibit GC *in vivo*

The therapeutic effects of DSF/Cu and Cu-EXO in GC mouse models were further investigated by dividing the mice into five groups. These groups were constructed with AGS cells and overexpressing *FDX1* of AGS cells, then treated with DSF/Cu or Cu-EXO (**Figure 7A**). *In vivo* imaging results showed that Cu-EXO labeled with DiR dye injected into the subcutaneous skin of mice with GC led to consistent fluorescence intensity at the tumor site within 1 h, indicating sustained drug retention and release at the tumor site over time (**Figure 7B**). After injecting Cu-EXO into the tail veins of mice, fluorescence at the tumor site was shown to increase over time within 24 h, proving that Cu-EXO can accumulate at the tumor site (**Figure S13A, B**). After 3 weeks of treatment, mouse tumors were removed, which revealed that overexpression of *FDX1* and treatment with DSF/Cu and Cu-EXO effectively inhibited the growth of GC tumors (**Figure 7C, D**). In addition, mice treated with DSF/Cu and Cu-EXO exhibited less weight change compared to controls (**Figure 7E**). Analysis of mouse tumors by western blot demonstrated that DSF/Cu and Cu-EXO treatment following *FDX1* overexpression significantly increased the expression of *FDX1* and decreased the expression of *WDR43* (**Figure 7F–H**). HE staining of mouse tumors and organs confirmed that Cu-EXO effectively inhibited tumors with no apparent adverse effects on mouse organs, demonstrating good biosafety (**Figure S14A, B**). The Cu content in the main organs of the mice in the treatment group was not significantly higher than the control group, proving that DSF/Cu and Cu-Exo treatment did not cause destruction of Cu homeostasis and obvious systemic toxicity (**Figure S15A**). In addition, long-term feeding and monitoring of GC mice treated with the same treatment were performed and it was found that the long-term survival rate of mice in the Cu-EXO treatment group was higher compared to the control group (**Figure S15B**). The above experimental results proved that DSF/Cu and Cu-EXO have a good inhibitory effect on tumor growth in mice and better biocompatibility compared to Cu-EXO.

# Discussion

GC, a malignant tumor, is in urgent need of research for effective treatment strategies[24]. Cu is essential for eukaryotic life

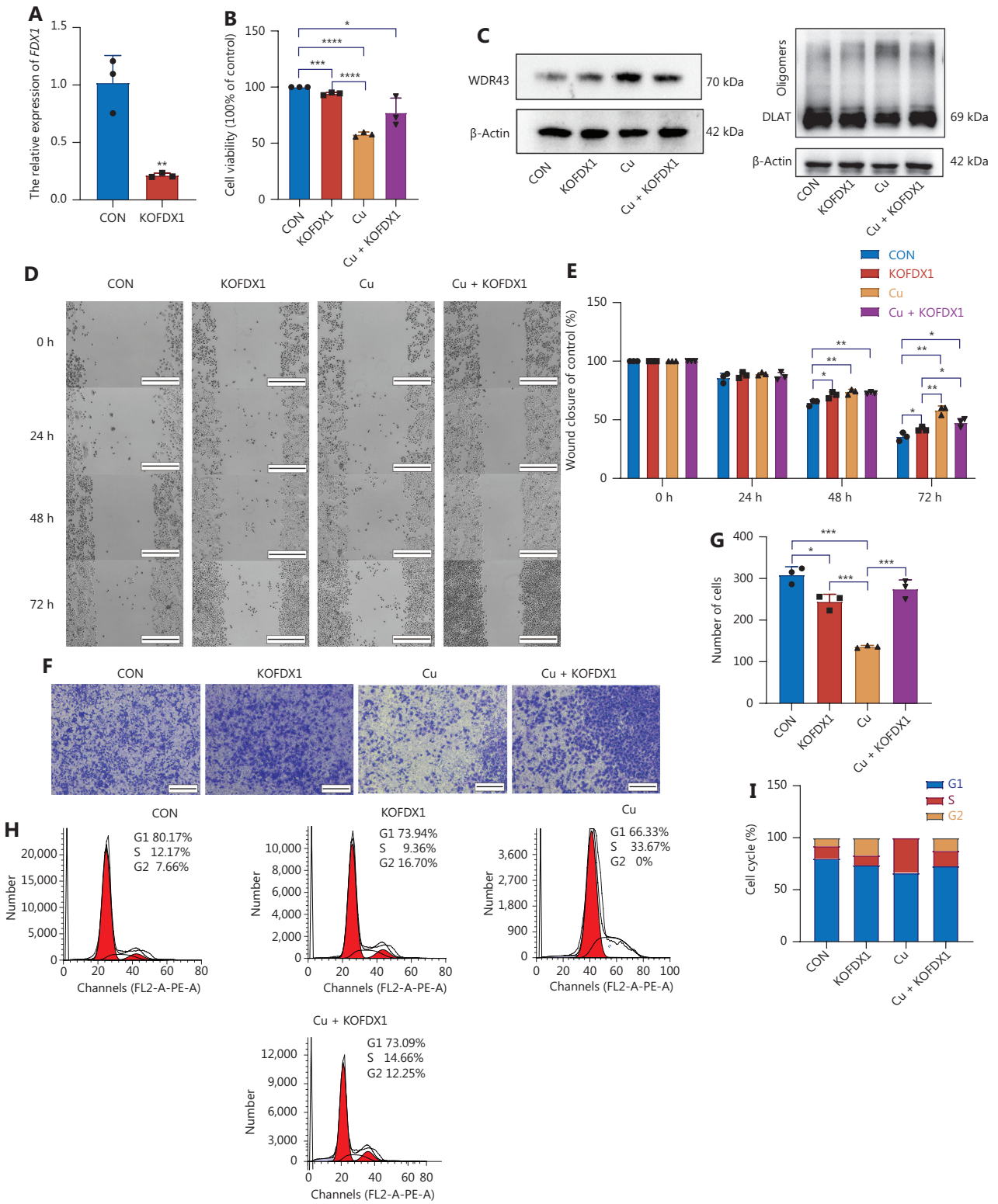



**Figure 4** Effect of *FDX1* knockout on GC cells. (A) qPCR was used to detect the level of *FDX1* gene in GC expression cells with *FDX1* knockout ($n$ = 3). (B) CCK-8 detected the proliferation of normal GC cells (CON), GC cells knocked out *FDX1* (KOFDX1), GC cells treated with 1 μM DSF/Cu for 24 h, and GC cells knocked out *FDX1*, then treated with DSF/Cu [Cu + KOFDX1] ($n$ = 3). (C) Western blot detection of the levels

of WDR43 and DLAT in GC cells after *FDX1* knockout ($n$ = 3). (D) Scratch healing assay to detect cell migration ($n$ = 3) (scale bar, 500 μm). (E) Statistical analysis of the results of scratch healing experiments ($n$ = 3). (F) Invasion assay to detect the invasion ability of cells ($n$ = 3) (scale bar, 100 μm). (G) Statistical analysis of the results of invasion experiments ($n$ = 3). (H) Cell cycle was measured by flow cytometry ($n$ = 3). (I) Statistical analysis of cell cycle test results ($n$ = 3). Data are expressed as the mean ± SD. *$P$ < 0.05, **$P$ < 0.01, ***$P$ < 0.001 and ****$P$ < 0.0001, indicating statistically significant differences.

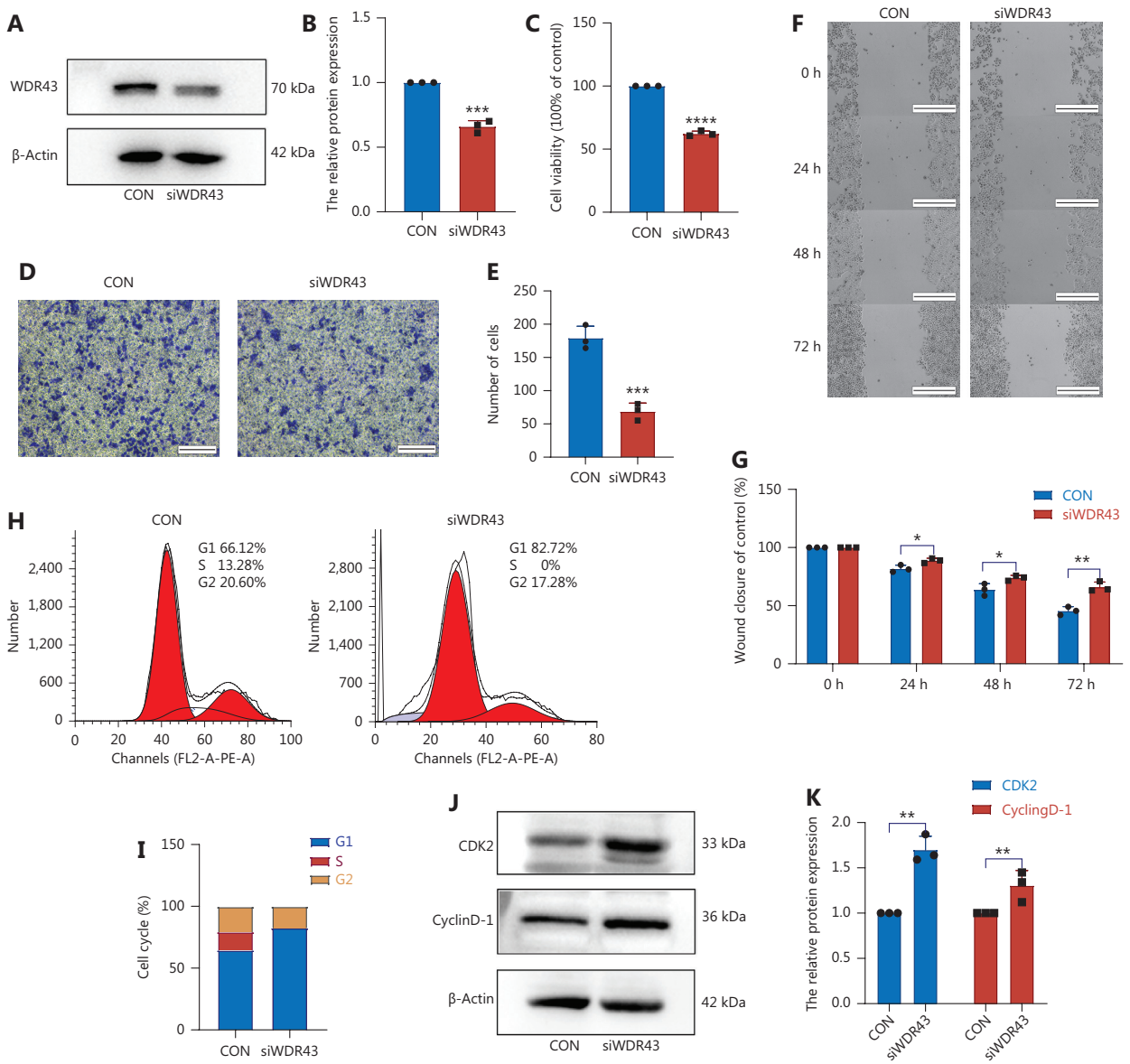



**Figure 5** Effect of *WDR43* knockdown on GC cells. (A) Western blot detection of WDR43 protein expression in GC cells with *WDR43* knockdown ($n$ = 3). (B) Statistical analysis of western blot. (C) CCK-8 detected the proliferation of non-treated GC (CON) and GC cells (siWDR43) after knocking down *WDR43* ($n$ = 3). (D) Invasion assay to detect the invasion ability of cells ($n$ = 3) (scale bar, 100 μm). (E) Statistical analysis of the results of the invasion experiment ($n$ = 3). (F) Scratch healing assay to detect cell migration ($n$ = 3) (scale bar, 500 μm). (G) Statistical analysis of the results of scratch healing experiments ($n$ = 3). (H) Cell cycle was measured by flow cytometry ($n$ = 3). (I) Statistical analysis of cell cycle test results ($n$ = 3). (J) Western blot analysis was performed to detect the levels of *CDK2*, *cyclinD-1*, and *DLAT* gene expression in GC cells with *FDX1* knockout ($n$ = 3). (K) Statistical analysis of western blot. Data are expressed as the mean ± SD. *$P$ < 0.05, **$P$ < 0.01, ***$P$ < 0.001, and ****$P$ < 0.0001, indicating statistically significant differences.

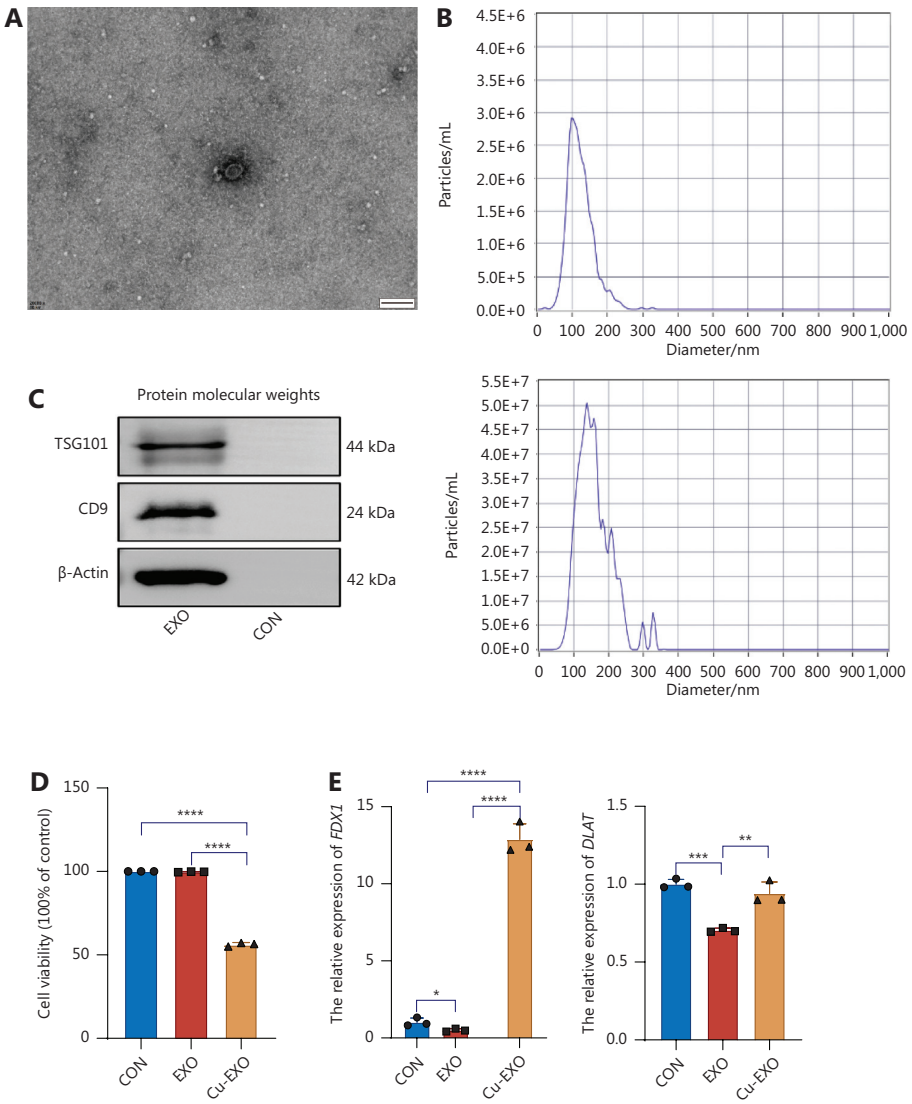



**Figure 6** Continued

processes but typically maintained at low cellular concentrations. Notably, moderate increases in Cu can lead to cytotoxicity and even cell death[25]. Moreover, tumor growth and metastasis are highly associated with Cu levels and significant changes are observed in the serum and tumor tissues of GC patients[26]. Intracellular Cu accumulation results in the aggregation of mitochondrial lipidized proteins and destabilization of Fe-S cluster proteins, ultimately leading to a unique form of cell death known as cuproptosis[27]. By inducing cuproptosis in GC cells, it is possible to inhibit cell proliferation, invasion, and metastasis *in vivo*. Given the crucial role of Cu in cancer progression, numerous Cu coordination compounds have been developed for anticancer treatment. Cu ionophores, like DSF, enhance Cu delivery into cells, thereby increasing intracellular Cu levels. There is more evidence proving that DSF has a good therapeutic effect on GC compared to elesclomol, which is often used in studies related to cuproptosis[28]. When combined with Cu ions, DSF may produce a better antitumor effect. The combination of DSF and Cu shows therapeutic potential against GC[14]. In addition, it has been shown that DSF/Cu can sensitize tumor cells to cisplatin by targeting aldehyde dehydrogenase (ALDH+), thereby reducing chemotherapy resistance in GC[29]. Therefore, we determined that DSF/Cu can inhibit GC and induce cuproptosis in GC cells. Our findings revealed that DSF/Cu treatment reduced the proliferation, migration, and invasion capabilities of GC cells, while also inducing cuproptosis. Analyzing the changes in the levels of genes associated with cuproptosis highlighted a potential link between GC treatment and the expression patterns of these genes.

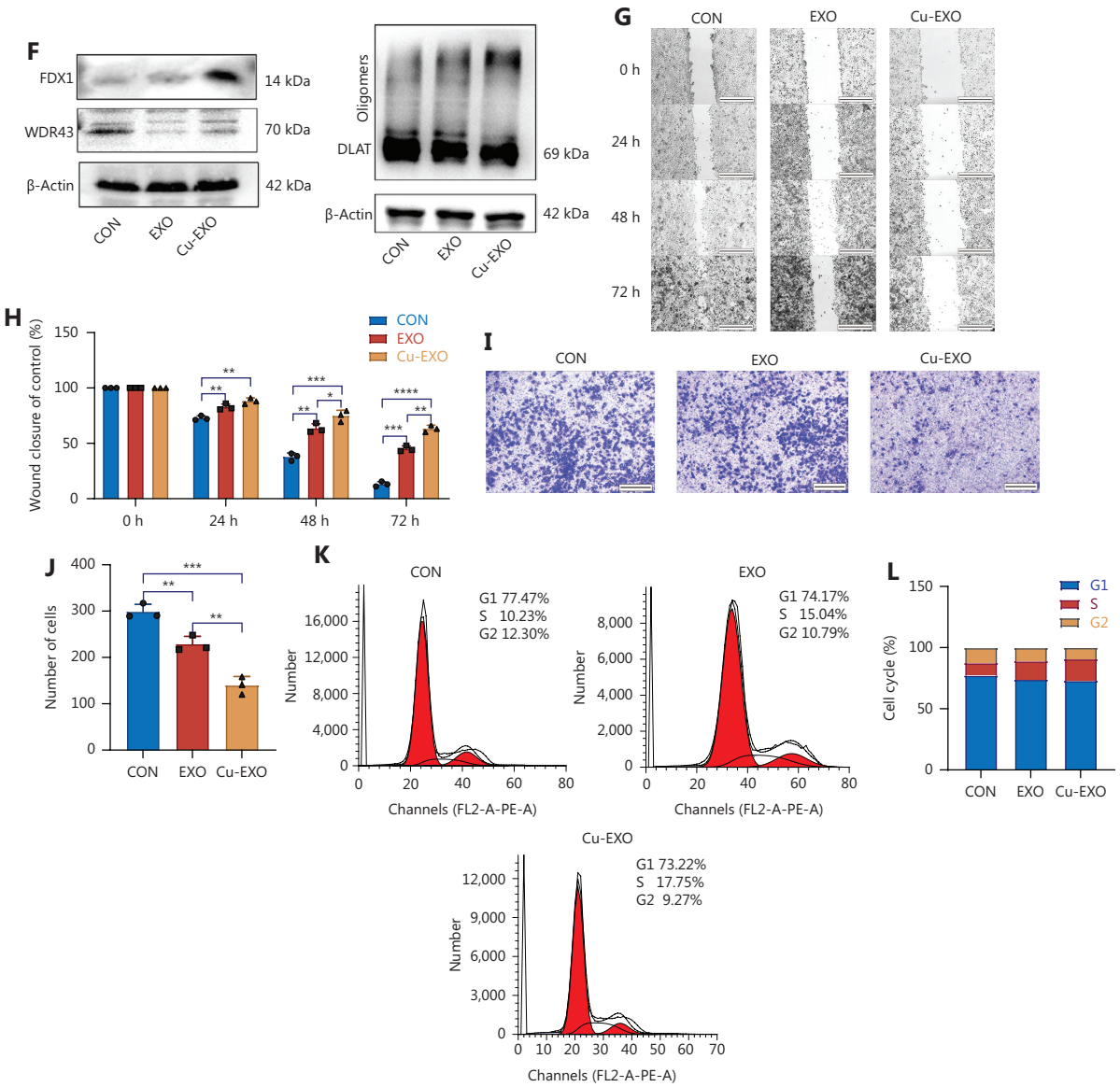



**Figure 6** DSF/Cu loaded into NK cell exosomes for the treatment of GC cells. (A) The morphology of NK cell exosomes was observed under transmission electron microscopy (scale bar, 200 nm). (B) Exosome particle size analysis of Cu-EXO. (C) Western blot detection of Cu-EXO exosome surface markers (TSG101 and CD9). (D) The proliferation of normal GC cells (CON), GC cells treated with 4 mg/mL of NK cell exosomes (EXO) for 24 h and GC cells treated with 4 mg/ml of DSF/Cu-loaded exosomes (Cu-EXO) for 24 h was detected by CCK-8 ($n$ = 3). (E) qPCR was used to detect the levels of *FDX1* and *DLAT* gene expression in Cu-EXO treated GC cells ($n$ = 3). (F) Western blot analysis of *FDX1*, *DLAT*, and *WDR43* gene expression in Cu-EXO treated GC cells ($n$ = 3). (G) Scratch healing assay to detect cell migration ($n$ = 3) (scale bar, 500 μm). (H) Statistical analysis of the results of scratch healing experiments ($n$ = 3). (I) Invasion assay to detect the invasion ability of cells ($n$ = 3) (scale bar, 100 μm). (J) Statistical analysis of the results of invasion experiments ($n$ = 3). (K) Cell cycle was measured by flow cytometry ($n$ = 3). (L) Statistical analysis of cell cycle test results ($n$ = 3). Data are expressed as the mean ± SD. $^{*}P < 0.05$, $^{**}P < 0.01$, $^{***}P < 0.001$, and $^{****}P < 0.0001$, indicating statistically significant differences.

Previous studies have demonstrated upregulation of most cuproptosis-related genes in GC tissues with a high mutation rate. Notably, the *FDX1* gene was shown to have a significant correlation with the survival rate of GC patients[30]. The *FDX1* gene can be used as a potential prognostic biomarker for GC patients and provide a new target for immune target therapy[4]. In addition, it has been confirmed that *FDX1* is responsible for reducing $Cu^{2+}$ to the more toxic $Cu^{1+}$ form and lactated

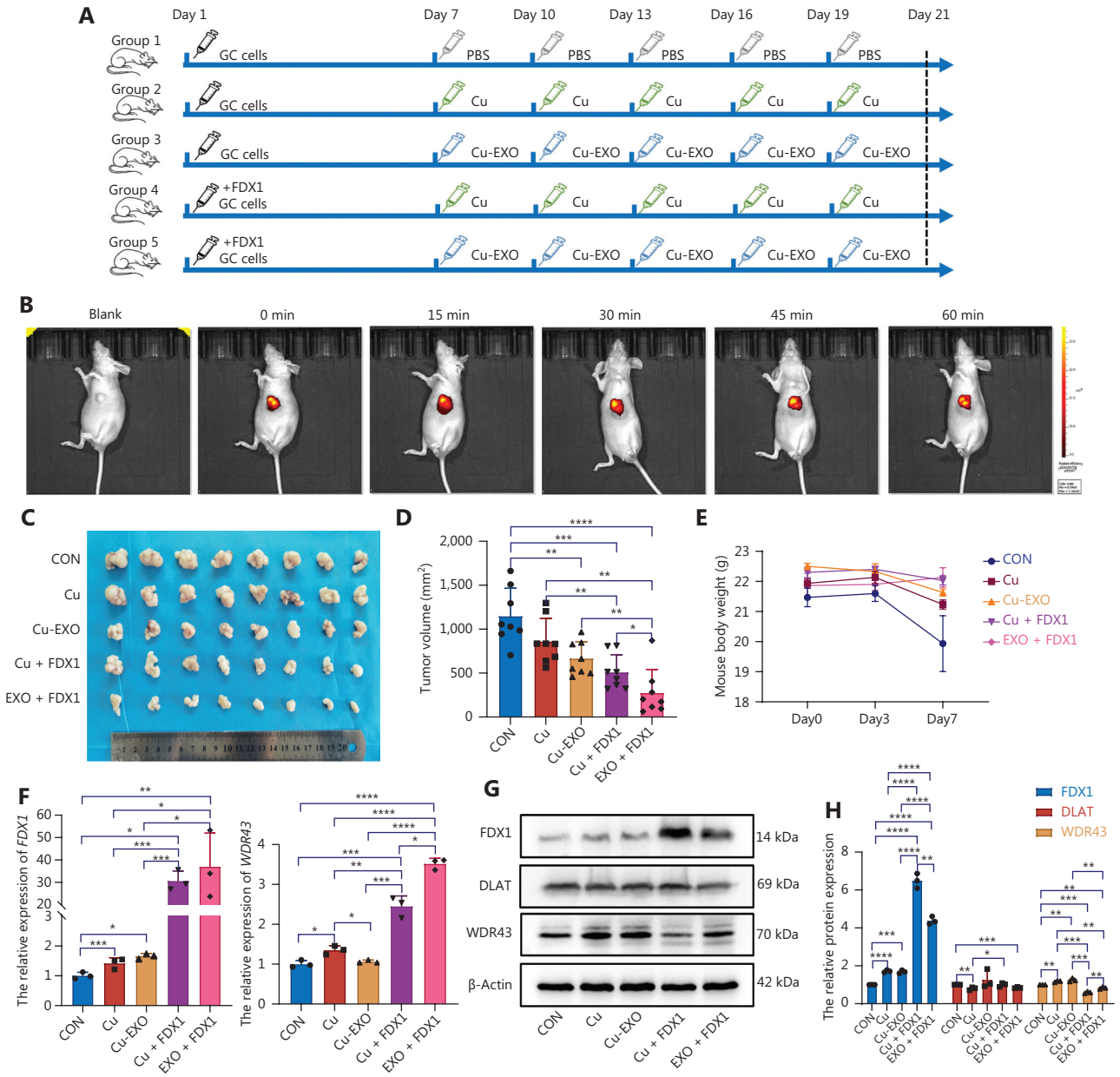



**Figure 7** DSF/Cu and Cu-EXO inhibit tumor growth *in vivo*. (A) Schematic diagram of experimental procedures in mice. The naked mice were divided into 5 groups ($n$ = 8), which were treated with PBS and DMSO after AGS tumor bearing (CON), 10 mg/kg of DSF/Cu after AGS tumor bearing (Cu), and 100 mg/kg of Cu-EXO after AGS tumor bearing (Cu-EXO). AGS cells overexpressing *FDX1* were treated with 10 mg/kg of DSF/Cu (Cu+FDX1) and 100 mg/kg Cu-EXO (EXO+FDX1). (B) *In situ* injection of DiR-labeled exosomes in nude mice and *in vivo* imaging detection. (C) Tumor volume in tumor-bearing mice ($n$ = 8). (D) Tumor volume analysis ($n$ = 8). (E) Weight changes in tumor-bearing mice after initiation of treatment ($n$ = 8). (F) The levels of *FDX1* and *WDR43* gene expression in mouse tumor tissues were detected by qPCR ($n$ = 3). (G) Western blot analysis of FDX1, DLAT, and WDR43 protein expression in mouse tumor tissues ($n$ = 3). (H) Statistical analysis of western blot. Data are expressed as the mean ± SD. *$P$ < 0.05, **$P$ < 0.01, ***$P$ < 0.001, and ****$P$ < 0.0001, indicating statistically significant differences.

METTL16 can modify FDX1 mRNA through m$^6$a, upregulating FDX1 mRNA and protein levels, and ultimately inducing cuproptosis in GC cells[31]. Therefore, we focused on the key *FDX1* gene to further explore the regulatory pathway that induces cuproptosis in GC cells. Our results showed that overexpression of *FDX1* causes more GC cells to develop cuproptosis. The results showed that compared to DSF/Cu treatment alone, the proliferation, migration and invasion ability of GC

cells overexpressing *FDX1* were significantly reduced after DSF/Cu treatment. Thus, increasing the expression of *FDX1* may be an important target to promote cuproptosis in GC cells.

In addition, protein sequencing of DSF/Cu-treated GC cells revealed the differentially expressed gene, *WDR43*, which was identified through bioinformatics analysis. Manipulating the levels of *FDX1* expression, either through deletion or overexpression, also altered *WDR43* expression. Specifically, increasing *FDX1* expression resulted in decreased WDR43 protein levels, thereby establishing a regulatory relationship between *FDX1* and *WDR43*. Previous research has indicated that *WDR43* is significantly overexpressed in colorectal cancer tissues with such overexpression associated with a poor prognosis in these patients. Moreover, knocking down *WDR43* substantially hinders cell growth by disturbing the cell cycle[8]. Similarly, our observations demonstrated that reducing *WDR43* expression in GC cells suppressed cell growth and disrupted the cell cycle. These findings highlight the critical role of *WDR43* in promoting cancer progression. Thus, this study provides evidence that the *FDX1*/*WDR43* axis has a role in inhibiting GC cell growth.

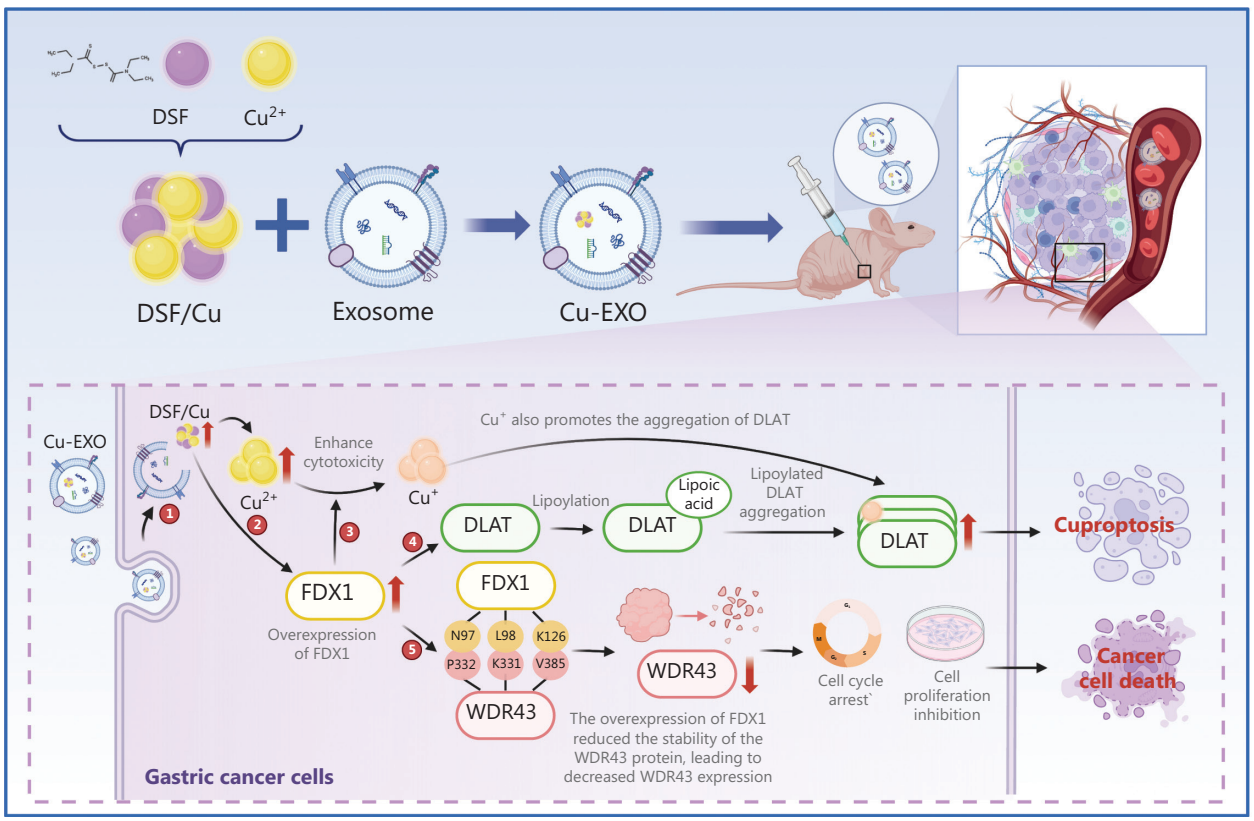



**Figure 8** Mechanism underlying NK cell exosome-mediated DSF/Cu delivery and induction of cuproptosis in gastric cancer (GC). Upper panel: Fabrication and *in vivo* application of the Cu-EXO nanocarrier. Disulfiram (DSF), a small-molecule aldehyde dehydrogenase inhibitor, and $Cu^{2+}$ were chelated at a 1:1 molar ratio and encapsulated into exosomes derived from natural killer (NK) cells. The resulting biomimetic Cu-EXO system exhibited enhanced biocompatibility and tumor-targeting capabilities, effectively suppressing tumor progression in GC murine models. Lower panel: Intracellular mechanisms underlying Cu-EXO-mediated cytotoxicity. Following cellular internalization (1), Cu-EXO releases the DSF/Cu complex, inducing intracellular copper accumulation (2) and activating ferredoxin 1 (FDX1), a mitochondrial iron-sulfur reductase. Acting as a central electron donor, FDX1 catalyzes the reduction of $Cu^{2+}$ to the highly cytotoxic $Cu^{+}$ (3) and facilitates the lipoylation of dihydrolipoamide S-acetyltransferase (DLAT), the E2 subunit of the pyruvate dehydrogenase complex, thus providing $Cu^{+}$-binding sites. Subsequent $Cu^{+}$ binding drives DLAT oligomerization, triggering profound proteotoxic stress and cuproptosis (4). Concurrently, FDX1 directly interacts with WD Repeat Domain 43 (WDR43), a scaffolding protein essential for ribosome biogenesis and cell proliferation *via* key structural residues (e.g., FDX1 N97–WDR43 P332) (5), which may facilitate the proteasomal degradation of WDR43 through uncharacterized, hypothetically ubiquitin-associated pathways, thereby inhibiting WDR43-driven oncogenic signaling that drives cell cycle progression and cell proliferation. Collectively, Cu-EXO drives robust GC cell death by converging the induction of DLAT-mediated cuproptosis and the targeted inhibition of WDR43. (Created with Biorender.com).

The Cu ionophore, DSF/Cu, has demonstrated efficacy in treating GC. However, the use of $Cu^{2+}$ poses risks due to the potential off-target toxicity, limiting the therapeutic potential. This research aims to develop a strategy to enhance the biocompatibility and safety of DSF/Cu treatment. Exosomes have a crucial role in the development and progression of various cancers and serve as effective carriers for delivering anti-cancer drugs[32]. NK cells eliminate target cells by releasing cytotoxic substances, like perforin, granulysin, and antimicrobial peptides[33]. To date, > 150 clinical trials have explored NK cell-based immunotherapies across various cancers, such as ovarian, breast, and non-small cell lung cancer[34]. However, these therapies have faced challenges in overcoming inherent limitations associated with cell-based treatments. Human NK cells release exosomes that are cytotoxic to tumor cells and activate immune cells[20]. NK cell-derived exosomes offer enhanced suitability for clinical applications. NK cell-derived exosomes can be customized for autologous use from individual patients and surpass whole cell-based therapies in terms of manufacturing, storage, transportation, and transplantation. Notably, NK exosomes can be reliably stored at −80°C for a minimum of 1 year, ensuring accessibility and stability. Utilizing exosomes instead of cells also mitigates certain risks typically associated with cell therapy[35]. Despite the potential of NK cell exosomes in cancer therapy, studies involving NK cell exosomes for GC treatment are limited. Thus, this study loaded DSF/Cu into NK cell exosomes to create Cu-EXO, which significantly suppressed the growth, migration, and invasion of GC cells. In a mouse model of GC, Cu-EXO inhibited tumor growth when *FDX1* was upregulated. It is worth noting that before exosomes are more widely applied in clinical practice, there are still many challenges to overcome, such as the standardization of exosome preparation, characterization, and quality control. To address some of these issues, the International Society for Extracellular Vesicles has proposed clear exosome standards (MISEV2014/2018)[36]. However, the transformation of exosomes into clinical treatments still requires the characterization of exosomes through standardized quantitative indicators, large-scale cell production, and environmental control to ensure that exosomes have the same quality in each isolation batch[37].

DSF/Cu can induce cuproptosis in GC cells with increased *FDX1* expression leading to higher rates of cuproptosis. Targeting the *FDX1*/*WDR43* axis could be a potential strategy for inhibiting the growth of GC cells. Moreover, using NK cell exosomes as carriers for DSF/Cu delivery in GC treatment may offer a safer approach. The discovery of cuproptosis opens up new possibilities for cancer therapy with gene expression related to cuproptosis having a critical role in cancer prevention and control. Understanding the mechanisms underlying cuproptosis and developing targeted therapies and gene treatments for GC are of significant clinical relevance.

# Conclusions

With the high incidence of GC in China accounting for approximately 50% of global cases, research on therapeutics and new molecular targets is crucial. Cuproptosis, a promising field, offers a novel approach to tumor treatment. Exosomes have also shown potential as effective carriers for therapeutic drugs in cancer treatment. This study delves into the cuproptosis induced by DSF/Cu delivered by exosomes from NK cells (**Figure 8**). Altering *FDX1* expression can enhance tumor sensitivity to DSF/Cu treatment, leading to improved efficacy at lower doses to minimize chemotherapy-related toxicities. Moreover, the elevated expression of *FDX1* can inhibit the expression of *WDR43*, thereby suppressing tumor progression. These findings hold significant clinical research implications and application possibilities.

# Acknowledgements

We appreciate all participants for their contributions.

# Grant support

This work was supported by the Jilin Province Science and Technology Development Program under Grant YDZJ202201ZYTS069, the Wenzhou Science & Technology Bureau Basic Public Welfare Research Program under Grant Y20240006, and the Jilin University Young Teachers and Students Cross-disciplinary Training Project under Grant 2023-JCXK-08.

# Conflict of interest statement

No potential conflicts of interest are disclosed.

# Author contributions

Conceived and designed the analysis: Qirong Li, Gongliang Guo, Dongxu Wang.
Collected the data: Qirong Li, Yi Guo, Jiahuan Yuan, Qiang Feng, Hengzong Zhou, Ming Hao, Boqiang Tao, Liqun Sun, Chao Lin, Jianfeng Mu, Gongliang Guo, Dongxu Wang.
Contributed data or analysis tools: Qirong Li, Yi Guo, Jiahuan Yuan, Qiang Feng, Hengzong Zhou, Ming Hao, Boqiang Tao, Liqun Sun, Chao Lin, Jianfeng Mu, Gongliang Guo, Dongxu Wang.
Performed the analysis: Qirong Li, Gongliang Guo, Dongxu Wang.
Wrote the paper: Qirong Li, Gongliang Guo, Dongxu Wang.

## Data availability statement

The data generated in this study are available upon request to the corresponding author.

## References


1. Ge EJ, Bush AI, Casini A, Cobine PA, Cross JR, DeNicola GM, et al. Connecting copper and cancer: from transition metal signalling to metalloplasia. Nat Rev Cancer. 2022; 22: 102-13.
2. Tsvetkov P, Coy S, Petrova B, Dreishpoon M, Verma A, Abdusamad M, et al. Copper induces cell death by targeting lipoylated TCA cycle proteins. Science. 2022; 375: 1254-61.
3. Xie J, Yang Y, Gao Y, He J. Cuproptosis: mechanisms and links with cancers. Mol Cancer. 2023; 22: 46.
4. Yan JN, Guo LH, Zhu DP, Ye GL, Shao YF, Zhou HX. Clinical significance and potential application of cuproptosis-related genes in gastric cancer. World J Gastrointest Oncol. 2023; 15: 1200-14.
5. Schapira M, Tyers M, Torrent M, Arrowsmith CH. WD40 repeat domain proteins: a novel target class? Nat Rev Drug Discov. 2017; 16: 773-86.
6. Sun H, Sun Q, Qiu X, Zhang G, Chen G, Li A, et al. WD repeat domain 43 promotes malignant progression of non-small cell lung cancer by regulating CDK2. Int J Biochem Cell Biol. 2022; 151: 106293.
7. Li Z, Feng M, Zhang J, Wang X, Xu E, Wang C, et al. WD40 repeat 43 mediates cell survival, proliferation, migration and invasion via vimentin in colorectal cancer. Cancer Cell Int. 2021; 21: 418.
8. Di Y, Jing X, Hu K, Wen X, Ye L, Zhang X, et al. The c-MYC-WDR43 signalling axis promotes chemoresistance and tumour growth in colorectal cancer by inhibiting p53 activity. Drug Resist Updat. 2023; 66: 100909.
9. Siegel RL, Miller KD, Fuchs HE, Jemal A. Cancer statistics, 2021. CA Cancer J Clin. 2021; 71: 7-33.
10. Wang Y, Zhang L, Yang Y, Lu S, Chen H. Progress of gastric cancer surgery in the era of precision medicine. Int J Biol Sci. 2021; 17: 1041-9.
11. Guan WL, He Y, Xu RH. Gastric cancer treatment: recent progress and future perspectives. J Hematol Oncol. 2023; 16: 57.
12. Skrott Z, Mistrik M, Andersen KK, Friis S, Majera D, Gursky J, et al. Alcohol-abuse drug disulfiram targets cancer via p97 segregase adaptor NPL4. Nature. 2017; 552: 194-9.
13. Liu W, Xiang H, Tan M, Chen Q, Jiang Q, Yang L, et al. Nanomedicine enables drug-potency activation with tumor sensitivity and hyperthermia synergy in the second near-infrared biowindow. ACS Nano. 2021; 15: 6457-70.
14. Liu Y, Guan X, Wang M, Wang N, Chen Y, Li B, et al. Disulfiram/Copper induces antitumor activity against gastric cancer via the ROS/MAPK and NPL4 pathways. Bioengineered. 2022; 13: 6579-89.
15. Zhou J, Yu Q, Song J, Li S, Li XL, Kang BK, et al. Photothermally triggered copper payload release for cuproptosis-promoted cancer synergistic therapy. Angew Chem Int Ed Engl. 2023; 62: e202213922.
16. Wu W, Yu L, Jiang Q, Huo M, Lin H, Wang L, et al. Enhanced tumor-specific disulfiram chemotherapy by *In Situ* $Cu^{2+}$ chelation-initiated nontoxicity-to-toxicity transition. J Am Chem Soc. 2019; 141: 11531-9.
17. Wu P, Zhang B, Ocansey DKW, Xu W, Qian H. Extracellular vesicles: a bright star of nanomedicine. Biomaterials. 2021; 269: 120467.
18. Krzewski K, Coligan JE. Human NK cell lytic granules and regulation of their exocytosis. Front Immunol. 2012; 3: 335.
19. Kang YT, Niu Z, Hadlock T, Purcell E, Lo TW, Zeinali M, et al. On-chip biogenesis of circulating NK cell-derived exosomes in non-small cell lung cancer exhibits antitumoral activity. Adv Sci (Weinh). 2021; 8: 2003747.
20. Wen C, Seeger RC, Fabbri M, Wang L, Wayne AS, Jong AY. Biological roles and potential applications of immune cell-derived extracellular vesicles. J Extracell Vesicles. 2017; 6: 1400370.
21. Lugini L, Cecchetti S, Huber V, Luciani F, Macchia G, Spadaro F, et al. Immune surveillance properties of human NK cell-derived exosomes. J Immunol. 2012; 189: 2833-42.
22. Xue Q, Kang R, Klionsky DJ, Tang D, Liu J, Chen X. Copper metabolism in cell death and autophagy. Autophagy. 2023; 19: 2175-95.
23. Chong W, Ren H, Chen H, Xu K, Zhu X, Liu Y, et al. Clinical features and molecular landscape of cuproptosis signature-related molecular subtype in gastric cancer. Imeta. 2024; 3: e190.
24. Smyth EC, Nilsson M, Grabsch HI, van Grieken NC, Lordick F. Gastric cancer. Lancet. 2020; 396: 635-48.
25. Chen L, Min J, Wang F. Copper homeostasis and cuproptosis in health and disease. Signal Transduct Target Ther. 2022; 7: 378.
26. Oliveri V. Selective targeting of cancer cells by copper ionophores: an overview. Front Mol Biosci. 2022; 9: 841814.
27. Tang D, Chen X, Kroemer G. Cuproptosis: a copper-triggered modality of mitochondrial cell death. Cell Res. 2022; 32: 417-8.
28. Cao Z, Hou Y, Zhao Z, Zhang H, Tian L, Zhang Y, et al. Reactivating Hippo by drug compounds to suppress gastric cancer and enhance chemotherapy sensitivity. J Biol Chem. 2024; 300: 107311.
29. MacDonagh L, Gallagher MF, Ffrench B, Gasch C, Breen E, Gray SG, et al. Targeting the cancer stem cell marker, aldehyde dehydrogenase 1, to circumvent cisplatin resistance in NSCLC. Oncotarget. 2017; 8: 72544-72563.
30. Wang J, Qin D, Tao Z, Wang B, Xie Y, Wang Y, et al. Identification of cuproptosis-related subtypes, construction of a prognosis model, and tumor microenvironment landscape in gastric cancer. Front Immunol. 2022; 13: 1056932.
31. Sun L, Zhang Y, Yang B, Sun S, Zhang P, Luo Z, et al. Lactylation of METTL16 promotes cuproptosis via $m^6a$-modification on FDX1 mRNA in gastric cancer. Nat Commun. 2023; 14: 6523.
32. Liu J, Ren L, Li S, Li W, Zheng X, Yang Y, et al. The biology, function, and applications of exosomes in cancer. Acta Pharm Sin B. 2021; 11: 2783-97.

33. Lettau M, Schmidt H, Kabelitz D, Janssen O. Secretory lysosomes and their cargo in T and NK cells. Immunol Lett. 2007; 108: 10-9.
34. Iliopoulou EG, Kountourakis P, Karamouzis MV, Doufexis D, Ardavanis A, Baxevanis CN, et al. A phase I trial of adoptive transfer of allogeneic natural killer cells in patients with advanced non-small cell lung cancer. Cancer Immunol Immunother. 2010; 59: 1781-9.
35. Shah NN, Baird K, Delbrook CP, Fleisher TA, Kohler ME, Rampertaap S, et al. Acute GVHD in patients receiving IL-15/4-1BBL activated NK cells following T-cell-depleted stem cell transplantation. Blood. 2015; 125: 784-92.
36. Théry C, Witwer KW, Aikawa E, Alcaraz MJ, Anderson JD, Andriantsitohaina R, et al. Minimal information for studies of extracellular vesicles 2018 (MISEV2018): a position statement of the International Society for Extracellular Vesicles and update of the MISEV2014 guidelines. J Extracell Vesicles. 2018; 7: 1535750.
37. Ma CY, Zhai Y, Li CT, Liu J, Xu X, Chen H, et al. Translating mesenchymal stem cell and their exosome research into GMP compliant advanced therapy products: promises, problems and prospects. Med Res Rev. 2024; 44: 919-38.

**Cite this article as:** Li Q, Guo Y, Yuan J, Feng Q, Zhou H, Hao M, et al. FDX1 expression promotes DSF/Cu-induced cuproptosis in gastric cancer cells. Cancer Biol Med. 2026; 23: 1320-1340. doi: 10.20892/j.issn.2095-3941.2025.0323